Materials Today Bio 14 (2022) 100251

Contents lists available at ScienceDirect

Materials Today Bio

journal homepage: www.journals.elsevier.com/materials-today-bio

Multifunctional polyphenol-based silk hydrogel alleviates oxidative stress and enhances endogenous regeneration of osteochondral defects

Wei Zhang [a,d,e,*], Yanan Zhang [a], Xiaolong Li [a], Zhicheng Cao [a,b], Qingyun Mo [a], Renwang Sheng [a], Chen Ling [a,b], Jiayu Chi [a], Qingqiang Yao [b,e,**], Jialin Chen [a,d,e,***], Hongmei Wang [a,c,****]

[a] School of Medicine, Southeast University, 210009, Nanjing, China
[b] Department of Orthopaedic Surgery, Institute of Digital Medicine, Nanjing First Hospital, Nanjing Medical University, 210006, Nanjing, China
[c] Department of Pharmaceutical Sciences, Binzhou Medical University, 264003, Yantai, Shandong, China
[d] Jiangsu Key Laboratory for Biomaterials and Devices, Southeast University, 210096, Nanjing, China
[e] China Orthopedic Regenerative Medicine Group (CORMed), China

ARTICLE INFO

Keywords:
Osteochondral regeneration
Hydrogel
Microenvironment
Oxidative stress
Tannic acid
Silk fibroin

ABSTRACT

In osteochondral defects, oxidative stress caused by elevated levels of reactive oxygen species (ROS) can disrupt the normal endogenous repair process. In this study, a multifunctional hydrogel composed of silk fibroin (SF) and tannic acid (TA), the FDA-approved ingredients, was developed to alleviate oxidative stress and enhance osteochondral regeneration. In this proposed hydrogel, SF first interacts with TA to form a hydrogen-bonded supramolecular structure, which is subsequently enzymatically crosslinked to form a stable hydrogel. Furthermore, TA had multiple phenolic hydroxyl groups that formed interactions with the therapeutic molecule E7 peptide for controlled drug delivery. In vitro investigations showed that SF-TA and SF-TA-E7 hydrogels exhibited a multitude of biological effects including scavenging of ROS, maintaining cell viability, and promoting the proliferation of bone marrow mesenchymal stem cells (BMSCs) against oxidative stress. The proteomic analysis indicated that SF-TA and SF-TA-E7 hydrogels suppressed oxidative stress, which in turn improved cell proliferation in multiple proliferation and apoptosis-related pathways. In rabbit osteochondral defect model, SF-TA and SF-TA-E7 hydrogels promoted enhanced regeneration of both cartilage and subchondral bone as compared to hydrogel without TA incorporation. These findings indicated that the multifunctional SF-TA hydrogel provided a microenvironment suitable for the endogenous regeneration of osteochondral defects.

1. Introduction

Articular cartilage is a transparent connective tissue covering the epiphyseal surface of articulating bones and protects subchondral bone from high pressure through effective load distribution. Cartilage defects and osteoarthritis (OA) are one of the most prevalent musculoskeletal diseases in clinical practice [1]. An osteochondral defect is the most severe cartilage defect (Grade IV), involving the defect to both articular cartilage and subchondral bone [2]. Due to the poor spontaneous repair capacity of cartilage, as well as the distinct biochemical and biomechanical properties of cartilage and subchondral bone, the repair of osteochondral defects is quite challenging [3]. Physiologically, when an osteochondral defect occurs and the subchondral bone plate is penetrated, a large number of endogenous bone marrow-derived mesenchymal stem cells (BMSCs) are released from the bone marrow and migrate into the chondral and subchondral areas to participate in the self-repair process [4]. However, the spontaneous repair process following trauma or microfracture surgery often results in the formation

* Corresponding author. School of Medicine, Southeast University, 210009, Nanjing, China.
** Corresponding author. Department of Orthopaedic Surgery, Institute of Digital Medicine, Nanjing First Hospital, Nanjing Medical University, 210006, Nanjing, China.
*** Corresponding author. School of Medicine, Southeast University, 210009, Nanjing, China.
**** Corresponding author. School of Medicine, Southeast University, 210009, Nanjing, China.
E-mail addresses: zhang.wei@seu.edu.cn (W. Zhang), yaoqingqiang@njmu.edu.cn (Q. Yao), jialin.chen@seu.edu.cn (J. Chen), wanghongmei85@163.com (H. Wang).

https://doi.org/10.1016/j.mtbio.2022.100251
Received 22 December 2021; Received in revised form 8 March 2022; Accepted 31 March 2022
Available online 9 April 2022

of fibrotic tissue, which is mechanically- and functionally-inferior to normal hyaline cartilage and subchondral bone [5,6].

A crucial reason for the adverse tissue repair is the presence of oxidative stress in the microenvironment during cartilage injury and degeneration. Under normal circumstances, low levels of reactive oxygen species (ROS) are produced in articular chondrocytes to maintain cartilage homeostasis by regulating cell apoptosis, gene expression, and ECM production [7]. When articular cartilage is damaged, the pathological acceleration of tissue metabolism and the continuous abnormal strain on the joint cause chondrocytes to produce abnormal levels of ROS through nicotinamide adenine dinucleotide phosphate (NADPH) oxidase [8]. Oxidative stress occurs when there are elevated intracellular levels of ROS, leading to cellular damage, apoptosis, ECM destruction, and thereby impairing cartilage homeostasis and regeneration [7,9–11]. To promote the regeneration of osteochondral defects, it is highly desirable to create a supportive microenvironment that improves the spontaneous repair process by recruiting endogenous BMSCs, maintaining cell viability, and reducing the harmful effects of oxidative stress.

Tissue engineering has emerged as a promising treatment method for osteochondral defects, since it combines biomaterials and biomolecules to provide a modified local microenvironment for endogenous self-repair [12]. Silk fibroin (SF) of *Bombyx mori* (*B. mori*) silkworm, a U.S. Food and Drug Administration (FDA)-approved biomaterial, has been widely used in tissue engineering applications due to its wide range of properties including good biocompatibility, excellent mechanical strength, adjustable degradation, and non-inflammatory by-products [13–15]. Among the multiple SF scaffolds developed for osteochondral tissue engineering, SF hydrogels have gained considerable attention due to their high-water content and 3D porous structure which are similar to the natural extracellular matrix (ECM) [16,17]. Previous studies have shown that functionalized SF hydrogels could regulate stem cell behaviors such as cell migration, proliferation, and differentiation [18,19]. Although each hydrogel shows beneficial effects on its specific purpose, there is still a lack of hydrogel with multifunctional properties that can provide a favorable microenvironment for osteochondral regeneration.

In recent years, the application of the FDA-approved drug tannic acid (TA) in biomedicine has received extensive attention. TA is a polyphenol molecule found in many plants, showing intrinsic biological properties such as antioxidation, antibacterial and anti-inflammatory effects [20–22]. In addition, TA contains multiple phenolic hydroxyl groups, which endow TA to form networks with other polymers such as biomaterials and peptides through hydrogen bonds, coordination bonds, and hydrophobic interactions [23,24]. Recently, we have developed a TA-mediated E7/P15 peptide-functionalized alginate hydrogel, in which TA acts as a reactive intermediate between alginate and peptides. The prime-coating of TA onto alginate hydrogel could enhance peptide conjugation and sustain the controlled release of pro-migratory and pro-differentiating peptides, ultimately improving osteochondral regeneration [25]. This study reported for the first time the application of TA in osteochondral defect repair; however, whether the TA functionalized hydrogel itself stimulates osteochondral repair without bioactive molecules, by regulating the microenvironment through reducing oxidative stress, has not yet been evaluated.

In the current study, we aim to develop a multifunctional hydrogel composed of SF and TA, the FDA-approved ingredients, to alleviate oxidative stress for enhanced osteochondral regeneration (Scheme 1). Although previous studies have fabricated SF-TA hydrogel as surgical sealants for hemostasis and wound healing [20,26–28], there are no studies that evaluate the effect of applying multifunctional SF-TA hydrogel on the regeneration osteochondral defects. In our developed SF-TA hydrogel, SF first interacts with TA to form a hydrogen-bonded supramolecular structure, which is subsequently enzymatically cross-linked to form a stable hydrogel with enhanced viscosity and hydrophilicity beneficial for osteochondral regeneration. Furthermore, TA has multiple phenolic hydroxyl groups that formed interactions with therapeutic molecule for controlled drug delivery. E7 (EPLQLKM), a recently identified BMSC-specific affinity peptide, was selected to be incorporated into the SF-TA hydrogel to recruit endogenous BMSCs [29,30]. SF-TA hydrogel shows ability to scavenge ROS, thereby maintaining cell viability, and promoting the proliferation of endogenous BMSCs against oxidative stress at the defect site. Global proteomic analysis was performed to further investigate the effects of SF-TA hydrogel on BMSCs as well as the underlying mechanisms. Lastly, in vitro osteochondral defect model was used to evaluate its biological performance on cartilage and subchondral bone regeneration. The developed multifunctional SF-TA hydrogel thus provides a supportive microenvironment, with a unique combination of properties, for endogenous regeneration of osteochondral defects and may serve as a promising biomaterial for future clinical treatment aimed at improving the endogenous healing of osteochondral defects.

2. Materials and methods

2.1. Fabrication of SF-TA hydrogel

SF solution was prepared by the method previously reported [31,32]. 8% (w/v) SF solution and 1% (w/v) TA solution (Sigma-Aldrich, St. Louis, MO) were mixed for final concentrations of 4% (w/v) and 0.005% (w/v) respectively. To initiate gelation, 20 U/ml horseradish peroxidase (HRP, type VI, Sigma-Aldrich, St. Louis, MO) and 0.01% (w/w) H_2O_2 (Yuanle, Shanghai, China) were added to the SF-TA solution, and mixed by gentle pipetting before setting [33]. For SF-TA-E7 hydrogel, 100 μg/ml of E7 peptide (EPLQLKM, Scilight-Peptide, Beijing, China) was added to the SF-TA solution before enzymatic crosslinking. The mixed solution was allowed to react at 25 °C or 37 °C and the gelation time was recorded. For animal study and cell experiments, TA, HRP and H_2O_2 solutions were sterile filtered using 0.45 μm polyvinylidene fluoride (PVDF) syringe filter (Millipore, USA), and hydrogels were sterilized with 75% (v/v) alcohol and stored at 4 °C before use.

2.2. Characterization of SF-TA hydrogel

The microstructure of the lyophilized hydrogels was observed by a Zeiss EVO 18 Scanning Electron Microscope (SEM, Carl-Zeiss, Oberkochen, Germany). The pore area of lyophilized hydrogels was measured from the SEM images (50 pores/group) using ImageJ software (NIH, Bethesda, MD). The porosity of hydrogels was calculated using the liquid displacement method as previously described [34]. The TA content in the hydrogel was determined using the Enhanced BCA Protein Assay Kit (Beyotime, China) as reported previously [25]. The pH value of the hydrogels was measured with a pH meter (INESA, Shanghai, China). The zeta potential of the hydrogels was evaluated with a Zeta Potential Analyzer (DT310, Dispersion Technology Instrument, USA). The pyrolysis characteristics of the hydrogels were evaluated using a TGA Q500 thermogravimetric analyzer (TA Instruments, New Castle, DE). The compressive modulus of SF and SF-TA hydrogels were evaluated using the compressive testing machine with a 50 N sensor (UTM2502; Sunstest, Shenzhen, China) as previously reported [25]. Rheological measurements including frequency sweep, strain sweep, and viscosity were performed using an MCR 302 rheometer (Anton Paar, Graz, Austria). The water contact angle of hydrogel surfaces was measured with an OSA 100 surface analyzer (LAUDA Scientific, Lauda-Königshofen, Germany). The equilibrium water content (EWC) of hydrogels was determined by measuring the weight of dry (Md) and wet (Mw) hydrogel before and

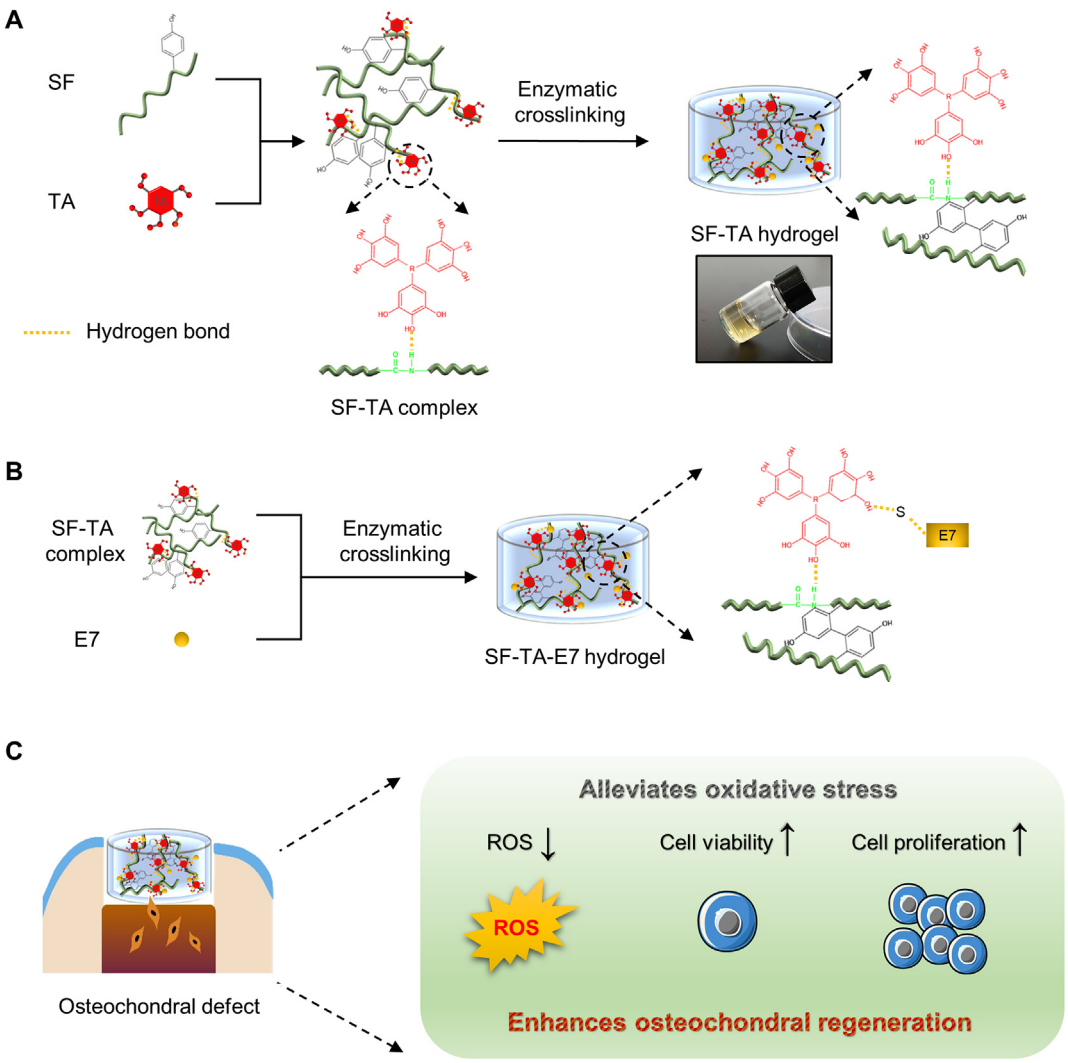

Scheme 1. Schematic illustration of the fabrication process and implementation of SF-TA hydrogel. (A) SF-TA hydrogel was prepared by pre-mixing SF and TA to form hydrogen bonds between them, followed by enzymatic crosslinking to covalently crosslink the tyrosine residues in SF to form dityrosine bonds. (B) E7 peptide was incorporated into SF-TA hydrogel and formed hydrogen bonds with TA. (C) After implantation of the SF-TA hydrogel into osteochondral defect, the hydrogel provides a supportive microenvironment to alleviate oxidative stress and enhance osteochondral regeneration.

after incubation in PBS for 24 h. EWC was calculated using the equation below:

$$EWC = (Mw\text{-}Md)/Mw$$

2.3. Fluorescence studies

To evaluate the molecular binding interactions between SF and TA, fluorometric titration experiments were performed by adding 0.005% (w/v) TA to 1% (w/v) and 4% (w/v) SF solution, as previously reported [27]. The fluorescence spectra of SF solution and SF-TA solution were recorded at λexc = 250 nm and λem from 270 to 550 nm on a Varioskan™ LUX multimode microplate reader (Thermo Fisher Scientific, Madison, WI). The fluorescence intensity at 305 nm was quantified for comparison between groups.

2.4. In vitro degradation

In vitro degradation of hydrogels was carried out by incubating the hydrogels in a simulated physiological environment (in PBS at 37 °C with shaking) [32]. The weight of dry hydrogel before (M0) and after (M1) degradation at each time point was recorded. The weight remaining was calculated using the equation below:

$$\text{Weight remaining } (\%) = M1/M0 \times 100$$

2.5. Controlled release profile

The evaluation of controlled release profile of hydrogels was performed as previously described [25,32,35]. Each hydrogel was incubated in 1 ml PBS at 37 °C with shaking. At each designated time point, 300 μl of supernatant fluid was collected and replaced with the same volume of fresh PBS for each sample. The concentration of FITC-labeled E7 released was measured by determining fluorescence intensities at 488/519 nm on a Varioskan™ LUX multimode microplate reader (Thermo Fisher Scientific, Madison, WI).

2.6. DPPH radical scavenging activity

The DPPH radical scavenging activity of hydrogels was measured as reported previously [36]. In brief, hydrogels were mixed with DPPH ethanol solution (2×10^{-4} mol/L, Shanghai Jinsui Bio-Technology, China), and incubated at 37 °C for 4 h. Consecutive spectra in the wavelength range of 400–600 nm was recorded on a Varioskan™ LUX

multimode microplate reader (Thermo Fisher Scientific, Madison, WI). The radical scavenging activity was measured by monitoring the absorbance at 517 nm, and calculated using the equation below:

$$\text{DPPH radical scavenging activity } (\%) = [(A_{Control} - A_{Sample})/ A_{Control}] \times 100$$

where $A_{Control}$ refers to the absorbance of the pure DPPH ethanol solution, and A_{Sample} refers to the absorbance of the DPPH solution in which the hydrogel is incubated.

2.7. Cell culture

Primary rat BMSCs (Cyagen Biosciences, Suzhou, China) were cultured in DMEM-low glucose media (Gibco, Carlsbad, CA) supplemented with 10% fetal bovine serum (FBS, Wisent, Canada) and 1% penicillin-streptomycin (Gibco, Carlsbad, CA) and placed in a humidified incubator at 37 °C with 5% CO_2. Media was changed every 3rd day until the cells reached confluence. Where indicated, 1 ng/ml IL-1β (Genscript, Nanjing, China) or 400 μM H_2O_2 (Yuanle, Shanghai, China) was added to the media to stimulate cells. Cell viability was measured with the Calcein-AM/PI Double Staining Kit (Dojindo, Japan), and cell proliferation was measured with Cell Counting Kit-8 (CCK8, APExBIO, Houston, TX), as described previously [5].

2.8. Intracellular ROS scavenging activity

Intracellular ROS scavenging ability of the hydrogels was studied by using the Reactive Oxygen Species Assay Kit (Beyotime Biotechnology, Beijing, China) according to the manufacturer's protocol. BMSCs were seeded into a 96-well plate and treated with 1 ng/ml IL-1β (Genscript, Nanjing, China) together with various hydrogel-conditioned media for 20 min. After the incubation, the cells were washed in PBS three times before adding the 2′, 7′-dichlorofluorescein-diacetate (DCFH-DA) probe, which can be oxidized by intracellular ROS to fluorescent dichlorofluorescein (DCF). DCF fluorescence in cells was observed and images were collected using fluorescence microscopy (Carl-Zeiss, Oberkochen, Germany). The fluorescence intensity was measured using ImageJ software (NIH, Bethesda, MD). Intracellular ROS scavenging activity was calculated from the ratio of the DCF fluorescence intensity of each hydrogel group to the IL-1β group.

2.9. Osteogenic and chondrogenic differentiation

Osteogenic and chondrogenic induction of BMSCs was performed according to our previous protocol [5]. Positive induction of osteogenesis was confirmed using BCIP/NBT Alkaline Phosphatase (ALP) Color Development Kit (Beyotime, China). Positive induction of chondrogenesis was confirmed using Alcian Blue staining (1%, pH = 2.5, Macklin, China). Quantification of staining intensity was performed using ImageJ software (NIH, Bethesda, MD).

2.10. Proteomic analysis

BMSCs were treated with SF, SF-TA or SF-TA-E7 hydrogel (n = 3/group) for 3 days and were extracted by lysis, followed by sonication and centrifugation. 200 μg protein samples from the cells were counted by BCA assay. Then, the protein samples were reduced by DTT and alkylated by iodoacetamide. All crude protein extracts were precipitated by acetone precipitation at −20 °C for 2 h, then the precipitated protein samples were re-dissolved in 200ul TEAB buffer. Finally, trypsin was added (trypsin/protein, 1:50), and the solution was incubated at 37 °C for 12–16 h. Digestion was stopped by the addition of 2% trifluoracetic acid. The tryptic digests were desalted with C18 solid-phase cartridges. Peptides were separated by HPLC focusing into 9 fractions.

Reverse-phase high-performance liquid chromatography (RP-HPLC) was performed. Briefly, the first dimension RP separation by micro-LC was performed on a U3000 HPLC System (Thermo Fisher Scientific, USA) by using a BEH RP C18 column (5 μm, 300 Å, 250 mm × 4.6 mm i.d., Waters Corporation, USA). The mass spectrometer was programmed to acquire in a data-dependent mode. The peptides were detected, isolated, and fragmented to produce a tandem mass spectrum of specific fragment ions for each peptide [37].

Mass spectra were analyzed using MaxQuant computational platform version 1.3.0.5 and Andromeda against the Uniprot FASTA rat database. The search included cysteine carbamidomethylation as a fixed modification and N-acetylation of protein and oxidation of methionine as variable modifications. A false discovery rate (FDR) of less than 0.01 for proteins and peptides and a minimum peptide length of 7 amino acids were required. Proteome quantification was performed in MaxQuant using the XIC based inbuilt label-free quantification (LFQ) algorithm. Label-free intensities were logarithmized and empty values were imputed with random numbers from a normal distribution, whose mean and standard deviation (SD) were chosen to best simulate low abundance values close to the noise level. The mass spectrometry proteomics data have been deposited to the ProteomeXchange Consortium (http://proteomecentral.proteomexchange.org) via the iProX partner repository with the dataset identifier PXD030026. Bioinformatic analysis was performed using DAVID, Cytoscape, and the OmicStudio tools at https://www.omicstudio.cn/tool. Only proteins with a p value of <0.05 were included within the gene ontology (GO) enrichment analysis and network formation.

2.11. Animal experiment

The animal experiment was performed according to the previous methods [25,32]. The study protocol was approved by the Animal Experimental Ethical Inspection Committee of Southeast University. Before surgery, SF, SF-TA, SF-E7 and SF-TA-E7 hydrogels (diameter: 5 mm, height: 4 mm) were prepared and maintained in the wet state. Adult male New Zealand white rabbits (~2.5 kg) were used and randomly divided (n = 3/group). After general anesthesia, the knee joint was opened with a medial parapatellar approach. The patella was dislocated laterally to expose the patellar groove. Osteochondral cylindrical defects (diameter: 5 mm, height: 4 mm) were created on the patellar groove on both the left and right limbs using an electric surgical drill, and then implanted with different hydrogels. After surgery, rabbits were allowed to move freely and fed with standard food and water. All the animals were sacrificed at 12 weeks post-operation.

2.12. Macroscopic and histological assessment

Samples of each group were examined with a stereo-microscope (SZ61, Olympus, Japan) for macroscopic evaluation according to the International Cartilage Repair Society (ICRS) macroscopic assessment scale, including “degree of defect repair”, “integration to border zone”, “macroscopic appearance”, and “overall repair assessment” subscores (Table S1) [38]. Samples were fixed in 4% (v/v) paraformaldehyde, and then decalcified in 10% (w/v) EDTA for 4 weeks under gentle shaking. After decalcifying, samples were embedded in paraffin and cut into 7 mm sections. Hematoxylin and eosin (H&E), safranine-O, and toluidine blue staining was performed for the evaluation of cell morphology and ECM production. Histological evaluation was performed based on an established histological scoring system, including cartilage evaluation (within the upper 1 mm of the defect), subchondral bone evaluation (within the bottom 2 mm of the defect) and total evaluation (Table S2) [39].

2.13. Micro-CT evaluation

Samples were scanned using a Micro-CT scanner (Bruker Sky-Scan1176, Billerica, MA), and high-resolution micro-CT images were collected. Reconstruction and analysis of bone volume/total volume (BV/TV), and trabecular numbers (Tb.N) were carried out by concentrically

placing a cylindrical region of interest (ROI, diameter: 5 mm, height: 5 mm) in the center of the original defect region with the threshold of 350–1080 for cartilage analysis, and >1080 for bone analysis [5].

2.14. Statistics

The quantitative data were presented as mean ± SD. Student's t-test was used when comparing 2 groups. One-way ANOVA with Tukey's multiple comparisons was performed when comparing between more than 2 groups. Differences were considered statistically significant at a p value of <0.05.

3. Results and discussions

3.1. Fabrication and characterization of SF-TA hydrogel

SF-TA hydrogels have previously been developed using high concentrations of TA to crosslink SF to allow the self-assembly into a hydrogel [26,27]. Bai et al. found that 30% (w/v) TA solution was able to co-assemble with SF to form a hydrogel sealant [26]. Jing et al. reported that TA with final concentrations from 0.1 to 0.7 wt % acted as a gelation binder to induce the gelation of SF by pH change, vortex, and gentle heating [27]. However, we and other groups have reported that high concentrations of TA had cytotoxicity [25,40,41]. Free TA with a concentration of >0.003% (w/v) was toxic to BMSCs, while 0.01% (w/v) TA-coated hydrogels showed good biocompatibility both in vitro and in vivo [25]. In this present study, SF-TA hydrogel was prepared by pre-mixing the 4% (w/v) SF and 0.005% (w/v) TA solutions followed by enzymatic crosslinking (Scheme 1A). To ensure its cytocompatibility, the concentration of TA used in this current system was within the safety limits and was significantly reduced as compared with the previously-reported SF-TA hydrogels [26,27]. The phenolic hydroxyl groups in TA form hydrogen bonds with amide groups in SF, resulting in a SF-TA complex with supramolecular network [24,25]. Due to the low TA concentration, this SF-TA complex did not self-assemble into a hydrogel, which is different from the previously-reported self-healing SF-TA hydrogels [26,27]. Hence, the purpose of using TA in the current system is to improve the biological activity of SF hydrogels rather than crosslinking. Subsequently, through the enzymatic reaction of HRP/H_2O_2, tyrosine residues in SF were covalently crosslinked to form dityrosine bonds, resulting in stable, highly elastic, and optically clear hydrogel (Scheme 1A) [33].

By gross observation, the pure SF hydrogel was colorless and transparent, while the SF hydrogel with TA incorporation was light yellow due to the color of TA molecule (Fig. 1A). By measuring the gelation time of the two hydrogels at different temperatures, it was observed that there was a significant difference in the gelation time of the two hydrogels at 25 °C (4.69 min for SF and 13.80 min for SF-TA, $p < 0.001$) and 37 °C (4.18 min for SF and 9.47 min for SF-TA, $p < 0.001$) (Fig. 1B). SF-TA hydrogels require longer gelation time than SF hydrogels, probably because the higher molecular weight of the SF-TA complex leads to an expanded spatial structure that decreases the interaction between the tyrosine residues of SF, thereby reducing the enzymatic crosslinking density and slowing down the gelation of SF hydrogel. The acquired SEM images of the freeze-dried hydrogels showed that the SF and SF-TA hydrogels were both highly porous, and the pores were interconnected and homogeneous (Fig. 1C). This interconnected porous structure is beneficial for defect repair because it could facilitate the transportation of nutrients and oxygen between the pores, as well as enhance cell distribution and tissue ingrowth [42]. The pore area of the SF-TA hydrogel ($25.33 \pm 7.40 \times 10^2$ μm^2) was significantly lower than that of the SF hydrogel ($31.04 \pm 10.07 \times 10^2$ μm^2, $p < 0.01$) (Fig. 1D). However, the porosity of the hydrogel did not change significantly after the incorporation of TA (Fig. 1E). Additionally, TA had no significant effect on the pH value (Fig. 1F), but reduced the zeta potential of SF hydrogels (Fig. 1G).

The BCA assay indicated that 83.52%, i.e., 41.76 μg/ml TA was successfully incorporated into the SF-TA hydrogel. Through the thermogravimetric analysis (TGA), it was observed that the residual mass of SF-TA hydrogel was 46.70%, which was greater than that of SF hydrogel (43.28%), indicating that TA has been incorporated into the SF-TA hydrogel (Fig. 1H). In addition, we used the fluorescence quenching method to evaluate the molecular binding interactions between SF and TA. Fluorescence emission spectra showed broad fluorescence peaks of SF (1% and 4%) with the peak maximum at 305 nm (Fig. 1I), due to the intrinsic fluorescence of SF protein. After TA was added, the fluorescence intensities of both 1% and 4% SF at 305 nm were obviously quenched resulting from the physical interactions between TA and SF molecules (Fig. 1I and J), as previously reported [27].

The mechanical properties of both SF and SF-TA hydrogels were evaluated by compressive and rheological tests. The SF hydrogel had a compressive modulus of 33.19 kPa, which is slightly higher than that of the SF-TA hydrogel (29.24 kPa), but no significant difference was detected (Fig. 1K). Rheological measurements were performed with SF and SF-TA hydrogels, as shown in Fig. 1L–N. The frequency sweeps of both SF and SF-TA hydrogels showed that the storage modulus (G′) was higher than the loss modulus (G″), and the G′ was $>10^3$ Pa in each case, indicating the formation of stable hydrogels (Fig. 1L). The strain sweeps revealed that the length of the linear-viscoelastic region (LVR) was not significantly altered by the incorporation of TA, while the flow point shifted from 12.12% in SF hydrogel to 15.90% in SF-TA hydrogel (Fig. 1M). Both frequency sweeps and strain sweeps indicated that the G′ of SF hydrogel was slightly higher than that of SF-TA hydrogel, indicating that TA incorporation decreased the mechanical strength of the hydrogel, which is consistent with the previous report [43]. As mentioned above, the incorporation of TA reduced the enzymatic crosslinking density and thus slightly decreased the mechanical properties of the SF hydrogel. Through the analysis of the viscosity of the two hydrogels, it was observed that the SF-TA hydrogel had higher viscosity than the SF hydrogel, since the TA in the SF-TA hydrogel had a large number of catechol groups which had strong dopamine-like adhesion [43] (Fig. 1N). The high viscosity of SF-TA hydrogel can provide good adhesion of the hydrogels to the tissue surface, which is beneficial for osteochondral regeneration since it can improve the integration of hydrogels with the host tissue at the defect site, and prevent the detachment of newly-formed cartilage [44,45].

The in vitro degradation behavior of SF and SF-TA hydrogels were compared in a simulated physiological environment (in PBS at 37 °C with shaking). In the course of 88 days, both hydrogels were slowly degraded and showed similar degradation curves (Fig. 1O). On day 88, the mass loss of SF hydrogel was about 15.78%, while that of SF-TA hydrogel was about 14.64%, but no significant difference was detected (Fig. 1O). The hydrophilicity of SF hydrogel and SF-TA hydrogel was evaluated by measuring the EWC and water contact angle of the two hydrogels. The data demonstrated that the EWC of SF-TA hydrogel was significantly higher than that of SF hydrogel (Fig. 1P), and the mean water contact angle of SF-TA hydrogel (68.9°) was smaller than that of SF hydrogel (84.8°) (Fig. 1Q), which collectively suggested that SF-TA hydrogel had better hydrophilicity. The large amount of phenolic hydroxyl groups in TA form strong hydrogen bonds with water, thereby increasing the hydrophilicity of SF-TA hydrogel [46]. Such enhanced hydrophilicity of hydrogel is beneficial for the absorption of bone marrow blood in the initial stage of osteochondral defect repair, which may improve the infiltration of BMSCs and growth factors into the hydrogel, and ultimately promote osteochondral regeneration [5].

E7 is a BMSC-specific affinity peptide, which has been identified with pro-migratory effect on BMSCs both in vitro and in vivo [29,30]. Besides, we and other groups have reported that the implantation of E7 peptide-functionalized scaffold enhanced endogenous osteochondral regeneration [25]. As observed from the in vitro scratch assay, the supplement of 100μg/ml E7 peptide into culture medium significantly improved BMSCs migration as compared to the control group, as

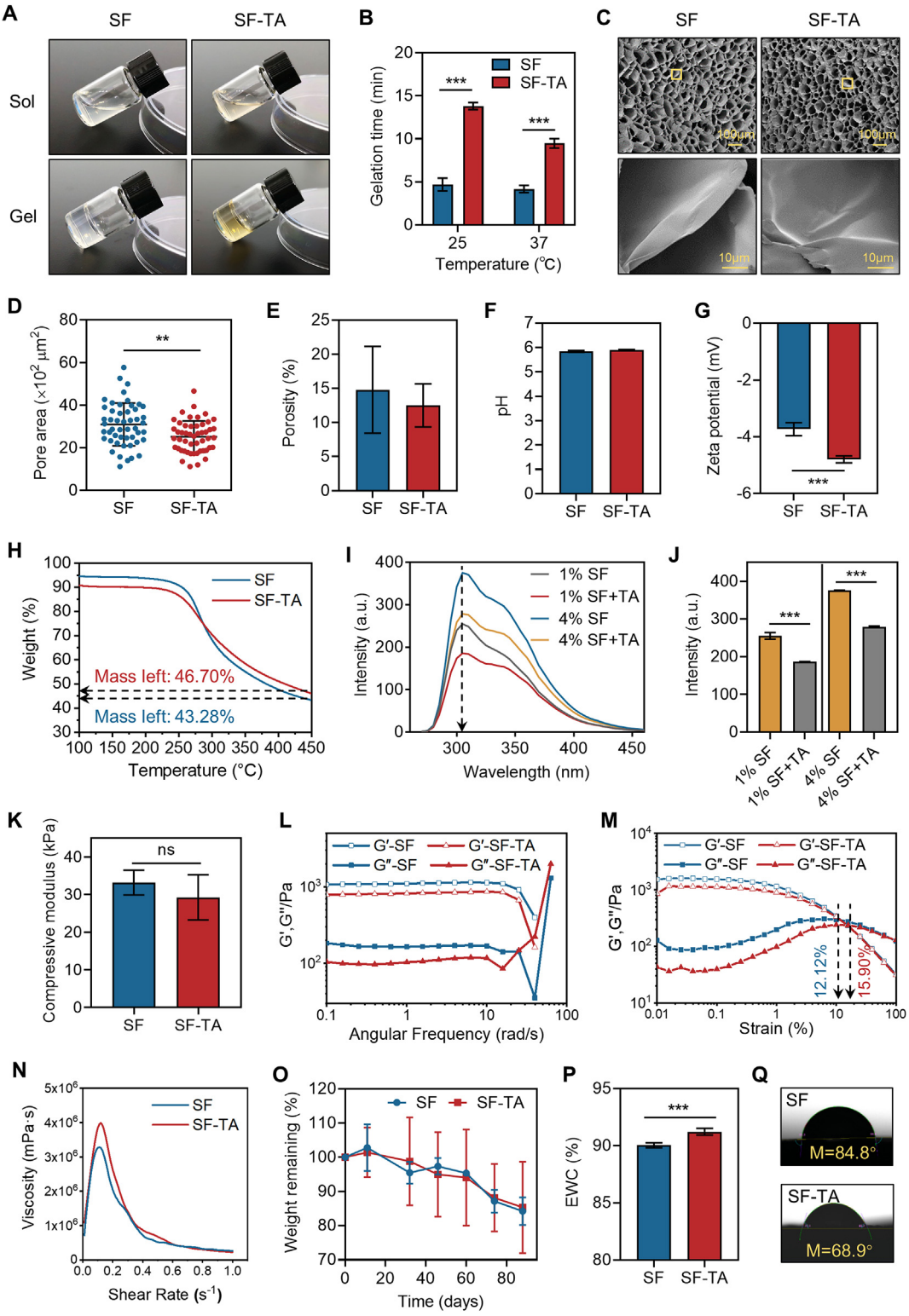

Fig. 1. Fabrication and characterization of SF-TA hydrogel. (A) Gross morphology of SF and SF-TA hydrogels before and after gelation. (B) Gelation time of SF and SF-TA hydrogels at 25 °C and 37 °C. (C) SEM images of lyophilized SF and SF-TA hydrogels. The lower panels represent higher magnification images (scale bars = 10 μm) of the corresponding orange boxes in the upper panels (scale bars = 100 μm). (D) Pore area of SF and SF-TA hydrogels. (E) Porosity of SF and SF-TA hydrogels. (F) pH value of SF and SF-TA hydrogels. (G) Zeta potential of SF and SF-TA hydrogels. (H) TGA plot of SF and SF-TA hydrogels. (I) Fluorescence emission spectra of 1% (w/v) and 4% (w/v) SF titrated with 0.005% (w/v) TA. (J) Quantitative comparison of the fluorescence intensity at 305 nm between groups. (K) Compressive modulus of SF and SF-TA hydrogels. (L) Frequency sweeps of SF and SF-TA hydrogels from 0.1 to 100 rad s^{-1} at 1% strain. (M) Strain sweeps of SF and SF-TA hydrogels from 0.01% to 100% strain at 10 rad s^{-1}. (N) Viscosity of SF and SF-TA hydrogels. (O) In vitro degradation curves of SF and SF-TA hydrogels in PBS at 37 °C. (P) Equilibrium water content of SF and SF-TA hydrogels. (Q) Water contact angle images of SF and SF-TA hydrogels. Results are shown as mean ± SD. **p < 0.01, ***p < 0.001.

evidenced by image analysis and migration area quantification (Fig. S1). After being incorporated into the SF-TA hydrogel, hydrogen bonds were formed between amino groups in E7 peptide and phenolic hydroxyl groups in TA (Scheme 1B). These interactions facilitated the controlled and sustained release of E7 from SF-TA hydrogel. In a simulated physiological environment (in PBS at 37 °C with shaking), the SF-TA hydrogel revealed a gradual release of E7 in more than 500 h (Fig. S2). As compared to SF hydrogel, the incorporation of TA into the SF-TA hydrogel inhibited the initial burst release and reduced the release for the remaining period. The ratio of E7 released from SF-E7 hydrogel and SF-TA-E7 hydrogel at day 21 was 63.92% and 43.84%, respectively (Fig. S2B). This is consistent with our previous study, where TA promoted the prolonged release of E7 from alginate-TA hydrogel [25].

3.2. Antioxidant activity and effect on cell viability of SF-TA hydrogel

In osteochondral defects, oxidative stress caused by changes in the microenvironment and elevated levels of ROS can disrupt the normal endogenous repair process [9]. In addition, the introduction of antioxidants into the defect may improve the repair of the osteochondral defect [47]. TA, the FDA-approved drug, is well-known to exert antioxidant activity; thus, the SF-TA hydrogel could be able to scavenge ROS and reduce the harmful effects of oxidative stress [20,27]. To evaluate the antioxidant activity of SF-TA hydrogel, we first measured the inhibitory effect of the hydrogels on DPPH free radicals. Following incubation for 150 min, the DPPH solution in the SF-TA and SF-TA-E7 hydrogel groups turned from purple to yellow, indicating that DPPH free radicals were scavenged in the solution (Fig. 2A). The radical scavenging activity was determined by measuring the absorbance decrease at 517 nm, revealing DPPH elimination rates of 76.34% and 67.61% for the SF-TA and SF-TA-E7 hydrogels, respectively, which were significantly higher than that of the SF hydrogel (35.86%, $p < 0.001$) (Fig. 2B and C).

We also evaluated the intracellular ROS by DCFH-DA, a probe that can detect ROS activity within the cell (Fig. 2D). Under fluorescence microscope, green fluorescence due to DCF was observed in BMSCs of the control group (without IL-1β), and the fluorescence intensity was strongly increased in the cells upon IL-1β stimulation. Proinflammatory cytokines such as IL-1β have been reported to increase ROS and mediate the pathogenesis of joint diseases [48]. The cells treated with IL-1β together with various hydrogel-conditioned media showed decreased DCF fluorescence as compared to the IL-1β group, while the TA-incorporated hydrogels (SF-TA and SF-TA-E7) substantially decreased the DCF fluorescence as compared to the pure SF hydrogel thus indicating efficient scavenging of intracellular ROS by TA. Further quantitative analysis also proved that SF-TA hydrogel had a significant ROS scavenging ability (Fig. 2E). The ROS scavenging ability of the SF-TA and SF-TA-E7 groups were significantly increased as compared to that of the SF group ($p < 0.001$). The highest ROS scavenging activity was shown by the SF-TA-E7 hydrogel with 95.52% inhibition relative to the IL-1β group, followed by SF-TA hydrogel with 89.94% of inhibition (Fig. 2E).

Since SF-TA hydrogel shows ability to scavenge ROS, we next evaluate whether it can protect BMSCs from oxidative stress-induced cell death. First, we evaluated the cell viability and proliferation under normal cell culture condition. Live/dead staining after 3 days of cell culture showed that the majority of the BMSCs cultured in each group remained viable, with healthy spindle shape of BMSCs (Fig. 2F). Microscopically, some dead cells could be observed in the SF group and negligeable number of dead cells in the SF-TA and SF-TA-E7 groups (Fig. 2F). According to the quantification of live and dead cells, the SF-TA and SF-TA-E7 groups showed viability of >95%, which was significantly higher than that of the SF group (89.16%, $p < 0.001$) (Fig. 2G). Cell proliferation was evaluated by CCK8 assay (Fig. 2H). In each group, the proliferation rate changed over time with a 4∼5-fold increase between day 1 and day 3. The proliferation rate of all groups was comparable on day 1. However, on day 3, the proliferation rates of the SF-TA and SF-TA-E7 groups were significantly higher than that of the SF group ($p < 0.01$ for SF-TA vs SF; $p < 0.001$ for SF-TA-E7 vs SF) (Fig. 2H).

Next, the influence of SF-TA hydrogel on cell viability and proliferation were investigated under more harsh cell culture conditions. Upon the stimulation of proinflammatory cytokines IL-1β, the cell viability of the SF group was reduced to 80.52%, and was significantly lower than those of the SF-TA group (87.01%, $p < 0.05$) and SF-TA-E7 group (89.02%, $p < 0.01$) (Fig. 2I and J). CCK8 assay revealed that as compred to the normal culture condition (Fig. 2H), BMSCs proliferation decelerated under the proinflammatory environment (Fig. 2K), as expected since IL-1β induces the generation of ROS which impedes cell proliferation [11]. The cell proliferation rate after 3 days of culture with SF-TA or SF-TA-E7 was still significantly higher than that of the SF group (Fig. 2K, $p < 0.001$). To better simulate the oxidative stress status, H_2O_2 was used to stimulate cells to promote the generation of intracellular ROS. Under the treatment of H_2O_2, fewer cells were observed compared with the normal culture condition, indicating the inhibitory effect of H_2O_2 on cell growth. All the three groups showed a decreased cell viability of ≤85%, but the SF-TA-E7 group had a significant higher cell viability (85.00%) as compred to the SF group (75.20%, Fig. 2L–M, $p < 0.01$). Similarly, CCK8 assay showed that the SF-TA-E7 group had the highest cell proliferation rate among the three groups (Fig. 2N). The above results indicated that SF-TA and SF-TA-E7 hydrogels significantly improved cell viability and proliferation against harmful oxidative stress, as compared to pure SF hydrogel. Previous studies have confirmed the pro-proliferative effect of E7 on BMSCs [49]. The mechanism by which TA increases cell viability and proliferation is to inhibit oxidative stress that induces cell death [7]. Interestingly, the SF-TA and SF-TA-E7 hydrogels showed comparable effect on cell viability and proliferation under normal or IL-1β-treated cell culture conditions (Fig. 2F–K); however, SF-TA-E7 hydrogel exhibited better effect than SF-TA on protecting BMSCs against the more harsh H_2O_2-stimulated condition (Fig. 2L–N). We speculated that the release of E7 form SF-TA-E7 hydrogel may strengthen the activity of antioxidant enzymes in the cells to modulate oxidative stress. This hypothesis needs to be tested in future studies. Additionally, as we mentioned above, it has been found that high concentrations of TA are cytotoxic [25,40,41], and therefore the concentration of TA should be adjusted so that it reduces ROS and induces cell proliferation but avoids cytotoxicity.

Previous studies have reported that the elevated levels of ROS inhibited osteogenic and chondrogenic differentiation of MSCs [10,50]; therefore, our developed SF-TA hydrogel may have the potential to improve BMSCs differentiation by scavenging ROS. The osteoinductive and chondroinductive abilities of SF-TA hydrogel on BMSCs were evaluated by representative staining assays. After being cultured in osteogenic media for 7 days, the SF, SF-TA, and SF-TA-E7 groups exhibited comparable ALP staining intensity (Fig. S3A). Similarly, alcian blue staining and quantitative analysis showed that after 14 days of culture in chondrogenic media, the TA incorporated hydrogels did not significantly enhance GAG deposition as compared to SF hydrogel (Fig. S3B). These results suggested that the incorporation of TA with/without E7 had no significant effect on BMSCs osteogenesis and chondrogenesis.

3.3. Proteomic analysis of SF-TA hydrogel on BMSCs

To gain a global view of the cellular activity and the affected signaling pathways of SF-TA hydrogel on BMSCs, LFQ-based proteomic analysis was performed, which identified 2167 proteins in total (Fig. S4, Table S3). The hierarchical clustering of differentially expressed proteins revealed significant changes in the expression level of 241 proteins (Fig. 3A, Table S4, $p < 0.05$). Principal component analysis (PCA) was performed on the proteomic data set of 9 samples, which revealed clear grouping of replicate samples for the SF, SF-TA or SF-TA-E7 groups, indicating similar protein expression between samples within a group (Fig. 3B). Venn diagrams showed the overlaps of significantly regulated proteins across each pairwise comparison against the SF group (Fig. 3C). The SF-TA and SF-TA-E7 hydrogels induced robust changes in the protein

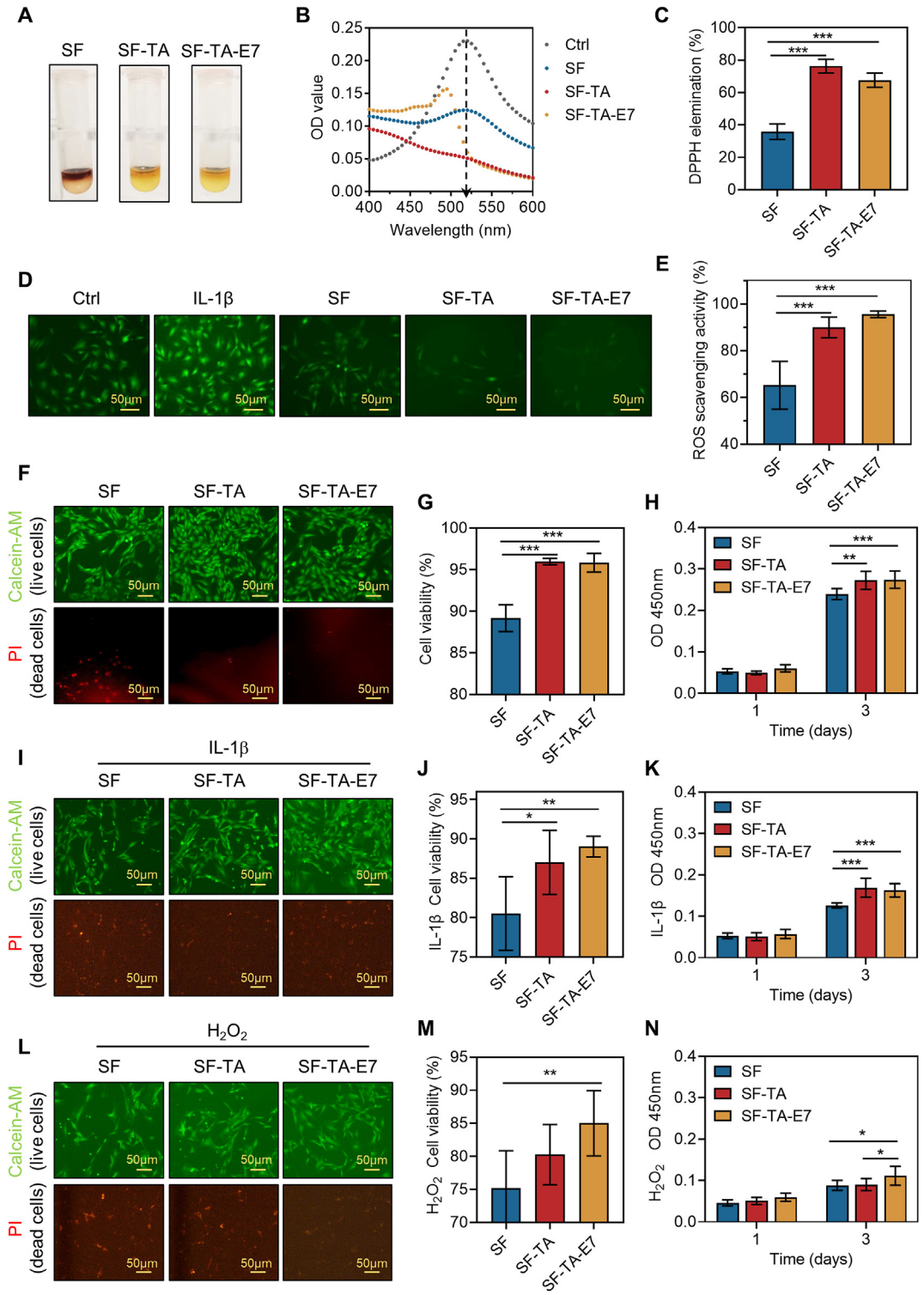

Fig. 2. Antioxidant activity and effect on cell viability of SF-TA hydrogel. (A) Gross view of SF, SF-TA, and SF-TA-E7 hydrogels in DPPH assay. (B) Consecutive spectra of DPPH solution with addition of different hydrogels in the wavelength range of 400–600 nm was recorded, and DPPH radical scavenging activity was measured by monitoring the absorbance at 517 nm. (C) DPPH radical scavenging activity of SF, SF-TA, and SF-TA-E7 hydrogels. (D) Fluorescence microscope images of DCF fluorescence in BMSCs treated with various hydrogel-conditioned media. Ctrl indicates control group (without IL-1β). Scale bars = 50 μm. (E) Intracellular ROS scavenging activity of SF, SF-TA, and SF-TA-E7 hydrogels. (F) Live/dead staining of BMSCs in normal cell culture condition for 3 days. Calcein-AM for live cells (green) and PI for dead cells (red). Scale bars = 50 μm. (G) Quantification of live/dead staining in normal cell culture condition. (H) CCK8 was used to detect the proliferation of BMSCs in normal cell culture condition for 1 and 3 days. (I) Live/dead staining of BMSCs in IL-1β-treated condition for 3 days. Scale bars = 50 μm. (J) Quantification of live/dead staining in IL-1β-treated condition. (K) CCK8 was used to detect the proliferation of BMSCs in IL-1β-treated condition for 1 and 3 days. (L) Live/dead staining of BMSCs in H_2O_2-treated condition for 3 days. Scale bars = 50 μm. (M) Quantification of live/dead staining in H_2O_2-treated condition. (N) CCK8 was used to detect the proliferation of BMSCs in H_2O_2-treated condition for 1 and 3 days. Results are shown as mean ± SD. *$p < 0.05$, **$p < 0.01$, ***$p < 0.001$.

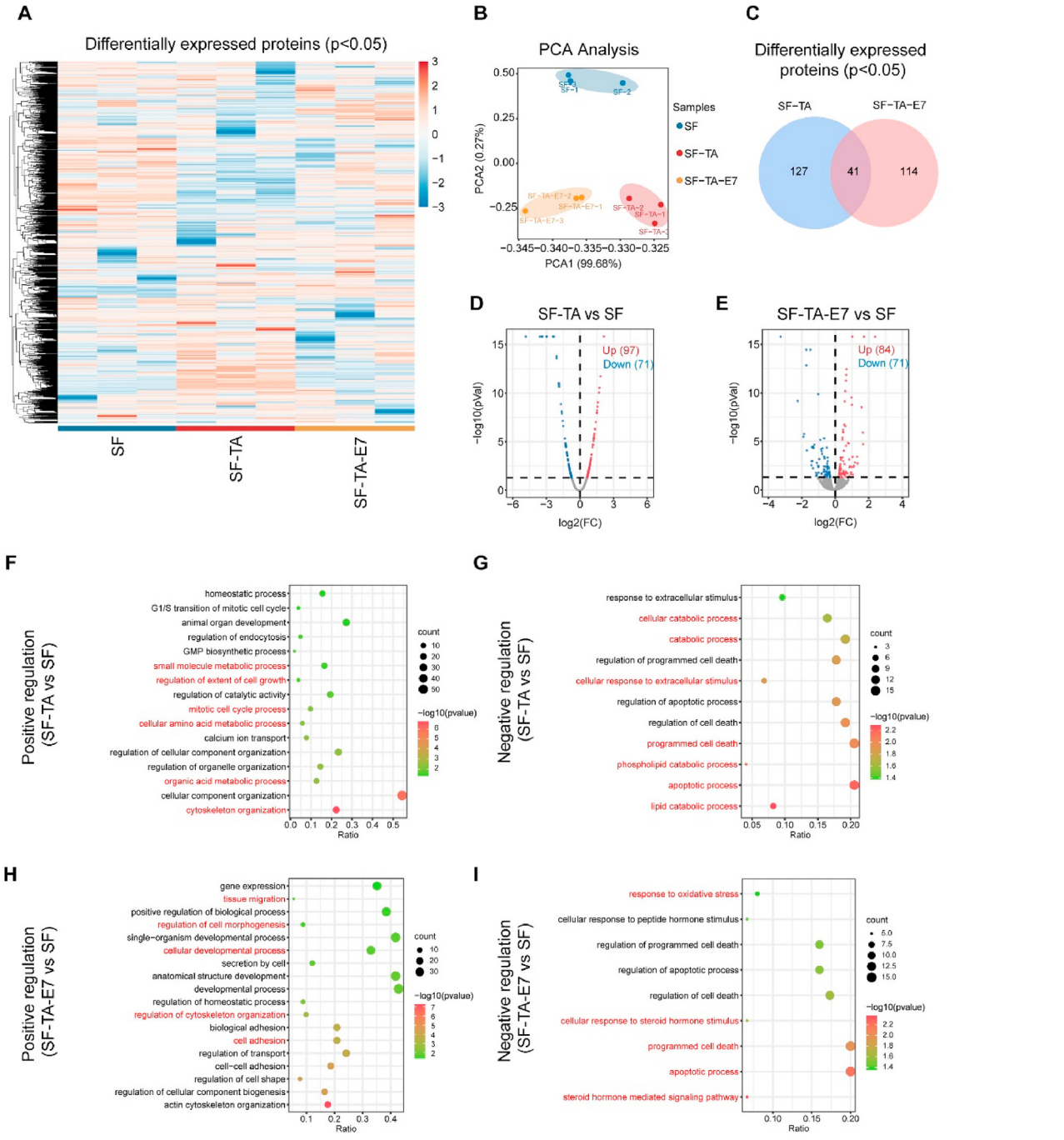

Fig. 3. Quantitative proteomic analysis revealing distinct protein signatures in different hydrogel groups. (A) Hierarchical clustering analysis of 241 LFQ-protein intensities (log2) that were quantified in three repeats of SF, SF-TA, and SF-TA-E7 groups and showed at least $p < 0.05$ in their abundance between at least two groups. Heatmap of z score- and log2-transformed LFQ protein intensities where proteins were grouped using unsupervised hierarchical clustering. (B) PCA plot of proteomic data with three groups and three biological replicates each. (C) Venn diagrams showing the overlaps of significantly regulated proteins across each pairwise comparison against the SF group. (D–E) Volcano plots compare three groups as indicated in the plot. Groups with p value < 0.05 were considered as significantly differential expression. The scatter plot depicts the difference score of these terms versus the −log10-transformed p value which is shown with red (UP) and blue (DOWN). (F–G) GO enrichment analysis for the category of up-regulated and down-regulated proteins between SF-TA and SF groups. (H–I) GO enrichment analysis for the category of up-regulated and down-regulated proteins between SF-TA-E7 and SF groups.

expression profile of BMSCs, with 168 and 155 differentially expressed proteins, respectively. The read count for protein expression was modeled by volcano plots to determine the expression profile among the groups. As shown in Fig. 3D, there were 97 up-regulated proteins and 71 down-regulated proteins between SF-TA and SF groups; while the SF-TA-E7 group showed fewer altered proteins which had 84 up-regulated proteins and 71 down-regulated proteins (Fig. 3E).

In order to determine the pathways significantly affected by SF-TA hydrogel, we utilized GO enrichment analysis to identify specific biological processes (BP). While SF-TA treatment showed enrichment for 396 GO terms ($p < 0.05$), SF-TA-E7 treatment resulted in 503 GO terms ($p < 0.05$). Under oxidative stress, high levels of ROS induce cellular damage and cell death [7]. For SF-TA group, as expected, the up-regulated proteins were mainly enriched in cell cycle, metabolic

processes, regulation of extent of cell growth, and cytoskeleton organization (Fig. 3F, Table S5), while the down-regulated proteins were significantly enriched in programmed cell death, apoptotic process, catabolic processes, and cellular response to extracellular stimulus, verifying that the antioxidant SF-TA hydrogel could enhance cell viability and proliferation (Fig. 3G, Table S5). Analysis of SF-TA-E7 vs SF revealed that the up-regulated proteins were significantly enriched in tissue migration, regulation of cell morphogenesis, cellular developmental process, and cell adhesion (Fig. 3H, Table S5); key terms specific to response to oxidative stress, programmed cell death, cellular response to steroid hormone stimulus and apoptotic process were negatively regulated which affected cell proliferation and cell viability in SF-TA-E7 group (Fig. 3I, Table S5). Steroid hormones regulate a wide variety of physiological and developmental functions. They have been shown to affect apoptosis and proliferation in osteoblasts, chondrocytes, cardiac cells, as well as cancer cells [51,52]. These GO enrichment analyses are consistent with the cell experiments that SF-TA and SF-TA-E7 hydrogels induced an enhanced effect on cell viability and cell proliferation as compared to SF hydrogel (Fig. 2F–H).

To further screen for the most significant hub proteins, an overview of regulated enriched protein sets is presented in Fig. 4A and B. We uploaded these hub proteins to the Cytoscape database for network analysis. The results in the SF-TA group demonstrated that the abundance links were directed to Guanine monophosphate synthase (GMPS), Exportin 1 (XPO1), Neural precursor cell expressed developmentally down-regulated protein 8 (NEDD8) and Cytoplasmic dynein complex 1 (DYNC1) family in the up-regulated proteins (Fig. 4A). GMPS and XPO1 are involved in the de novo synthesis of guanine nucleotides which are not only essential for DNA and RNA synthesis, but also provide GTP, which is involved in a number of cellular processes important for cell division [53]. XPO1 also affects oxidative stress by regulating STAT3 [54]. While NEDD8 promotes ubiquitination of proteins associated with apoptosis [55], DYNC1 family regulates apoptosis and autophagy of cells [56]. Taken together, these proteins show improvements in cell viability and proliferation, verifying the GO enrichment analysis that the most significant signature pathways of regulation of extent of cell growth, cytoskeleton organization, negative regulation of cell death and apoptotic process, and so on (Fig. 3F and G). We also showed these hub proteins of SF-TA-E7 group for a network that was related to cell proliferation, migration, cellular developmental process and so on (Fig. 4B). The Chaperonin Containing TCP1 (CCT) family proteins CCT2 and CCT5 were up-regulated, which are documented to promote mitotic cell cycle process and inhibit apoptotic process [57,58]. Except for CCT family, T-Complex 1 (TCP1), Protein phosphatase 1 catalytic subunit alpha (PPP1CA) and Poly(ADP-ribose) polymerase 1 (PARP1) also promote cell proliferation and migration [59,60]. Tropomyosin (TPM) family plays an important role in the growth of many tissues [61,62]. Myosin light chain (MYL) 9/12 has been reported to suppress inflammation by interacting with Cluster of differentiation 69 (CD69) in the recruitment of activated T cells into the inflammatory tissues [63,64], indicating the potential of SF-TA-E7 hydrogel in the modulation of inflammation.

Due to the limitations of differential expression proteomic analysis, we performed gene set enrichment analysis (GSEA) for all proteins, which is routinely used to analyze and interpret coordinate pathway-level changes. First, hub proteins with high connectivity were screened out from the brown module (Fig. 4C and D). As expected, GSEA of SF-TA group strongly implicated that pathways related to oxidative stress, such as response to oxygen radical, cellular oxidant detoxification, detoxification of reactive oxygen species, and NADH metabolic process were significantly down-regulated (Fig. 4C). Moreover, GSEA revealed cell cycle and cytoskeleton organization as the main biological process up-regulated by SF-TA treatment (Fig. 4C), Notably, Rho GTPase and MAPK pathway were up-regulated, which have been reported to regulate the cellular redox state and function in multiple biological processes, including cell growth, motility, polarity, and apoptosis [65,66]. In the SF-TA-E7 group, up-regulated pathways in the GSEA included cytoskeleton organization, cell morphogenesis involved in differentiation, positive regulation of cellular component organization, Rho GTPase and ROCK signaling (Fig. 4D). ROCK is a kind of Rho-associated kinase, originally identified as an effector of the small Rho GTPase, playing a variety of functions including the regulation of cell proliferation, morphology, contraction, motility, and polarity, etc [67].

Deep analysis of the proteomic data further evidenced that proliferation-related proteins and apoptosis-related proteins were significantly regulated with SF-TA or SF-TA-E7 treatment. Both SF-TA and SF-TA-E7 treatments promoted proliferation, but the proliferation-associated signaling pathways were different (Fig. 4E and F). For example, in SF-TA group, integrin-linked kinase (ILK) has multiple functions in cells, such as cell-extracellular matrix interactions, cell cycle, apoptosis, cell proliferation and cell motility, which are associated with the interacting partners of ILK and downstream signaling pathways [68]. Fatty acid synthase (Fasn) has been reported to affect cell proliferation and apoptosis [69]. Proprotein convertase subtilisin/kexin type 9 (PCSK9) regulates the NODAL signaling pathway and cellular proliferation in human induced pluripotent stem cells [70]. Topoisomerase I (TOP1MT) is required for mitochondrial DNA homeostasis and tissue regeneration [71]. Calcium/calmodulin-dependent protein kinase type II subunit delta (CAMK2D) enhances cell proliferation by combining non-coding RNA [72,73]. Meanwhile, in SF-TA-E7 group, MYH family and serine/arginine-rich splicing factor 2 (SRSF2) promote the proliferation, migration, invasion, and sphere formation of cells [74,75]. CAPZ family also controls cell survival and proliferation via regulating non-coding RNA [76].

Taken together, these proteomic analyses further verified that the SF-TA hydrogel suppressed oxidative stress and improved cell viability through multiple proliferation and apoptosis-related pathways; that is, providing a supportive microenvironment for osteochondral regeneration.

3.4. Effect of SF-TA hydrogel on osteochondral regeneration in vivo

The in vitro results indicate that the developed SF-TA hydrogel has a variety of biological properties, such as antioxidant activity, cell viability maintenance, pro-proliferative effects, and sustained release of the therapeutic molecule E7 which enhances cell migration. Lastly, we aim to investigate whether SF-TA hydrogel can regulate the microenvironment of osteochondral defects and enhance endogenous regeneration. SF, SF-TA, and SF-TA-E7 hydrogels were implanted into a rabbit osteochondral defect model, and the regenerative effect was compared (Fig. 5A). After 12 weeks of implantation, specimens were collected for macroscopic, micro-CT, and histological evaluation. The macroscopic images were shown in Fig. 5B and C. The defect area in SF group was larger than that of the other groups with a clear cavity in the center. The in vivo macroscopic results of the SF group are consistent with previous studies by ours or other groups that unfunctionalized SF scaffolds were not sufficient to promote osteochondral regeneration, possibly due to the lack of bioactivity of SF biomaterials [5,77]. The regenerated cartilage surface in SF-TA and SF-TA-E7 groups was superior to that of the SF group. The defect area in SF-TA group was filled with a large amount of white newly-formed tissue, and the repair was relatively complete. In SF-TA-E7 group, the cartilage surface was almost regenerated with small areas of cracks remained. After 12 weeks of implantation, the hydrogels in SF-TA and SF-TA-E7 groups degraded faster than those in SF group (Fig. 5C), although there was no significant difference between SF hydrogel and SF-TA hydrogel in the in vitro degradation experiment (Fig. 1O).

According to the ICRS scoring system, the score for “degree of defect repair” of SF group (2.58 ± 0.14) was significantly lower than those of SF-TA group (3.89 ± 0.19, $p < 0.001$) and SF-TA-E7 group (3.61 ± 0.19, $p < 0.001$) (Fig. 5D). The scores for “integration to border zone” of SF-TA group (4.00 ± 0.00) and SF-TA-E7 group (3.61 ± 0.10) were higher than that of SF group (3.08 ± 0.29, $p < 0.01$ for SF-TA vs SF; $p < 0.05$ for SF-

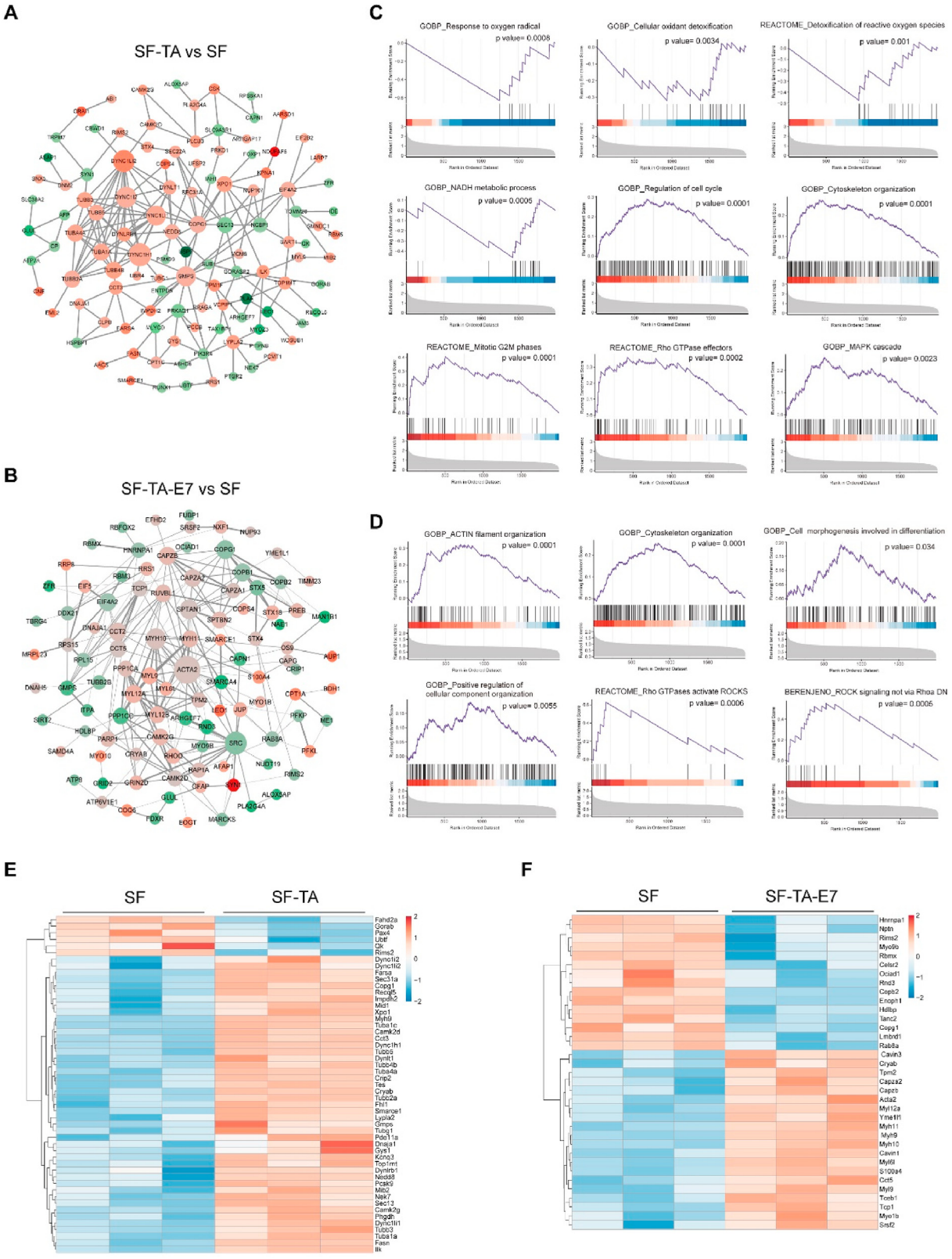

Fig. 4. Functional effects of the SF-TA hydrogels on BMSCs. (A) Network of differentially expressed proteins between SF-TA and SF groups. Red and green nodes indicate up-regulated and down-regulated molecules, respectively. (B) Network of differentially expressed proteins between SF-TA-E7 and SF groups. (C) SF-TA: GSEA of the proteins associated with oxidative phosphorylation, NADH metabolic process, Rho-GTPases, cytoskeleton organization, and cell proliferation related pathways. (D) SF-TA-E7: GSEA-enrichment plots of representative protein sets: cytoskeleton organization, cell morphogenesis involved in differentiation, cellular component organization, Rho-GTPases and ROCK signaling. (E–F): Heatmap of the distinct proliferation-related and apoptosis-related proteins of SF-TA vs SF, and SF-TA-E7 vs SF, respectively.

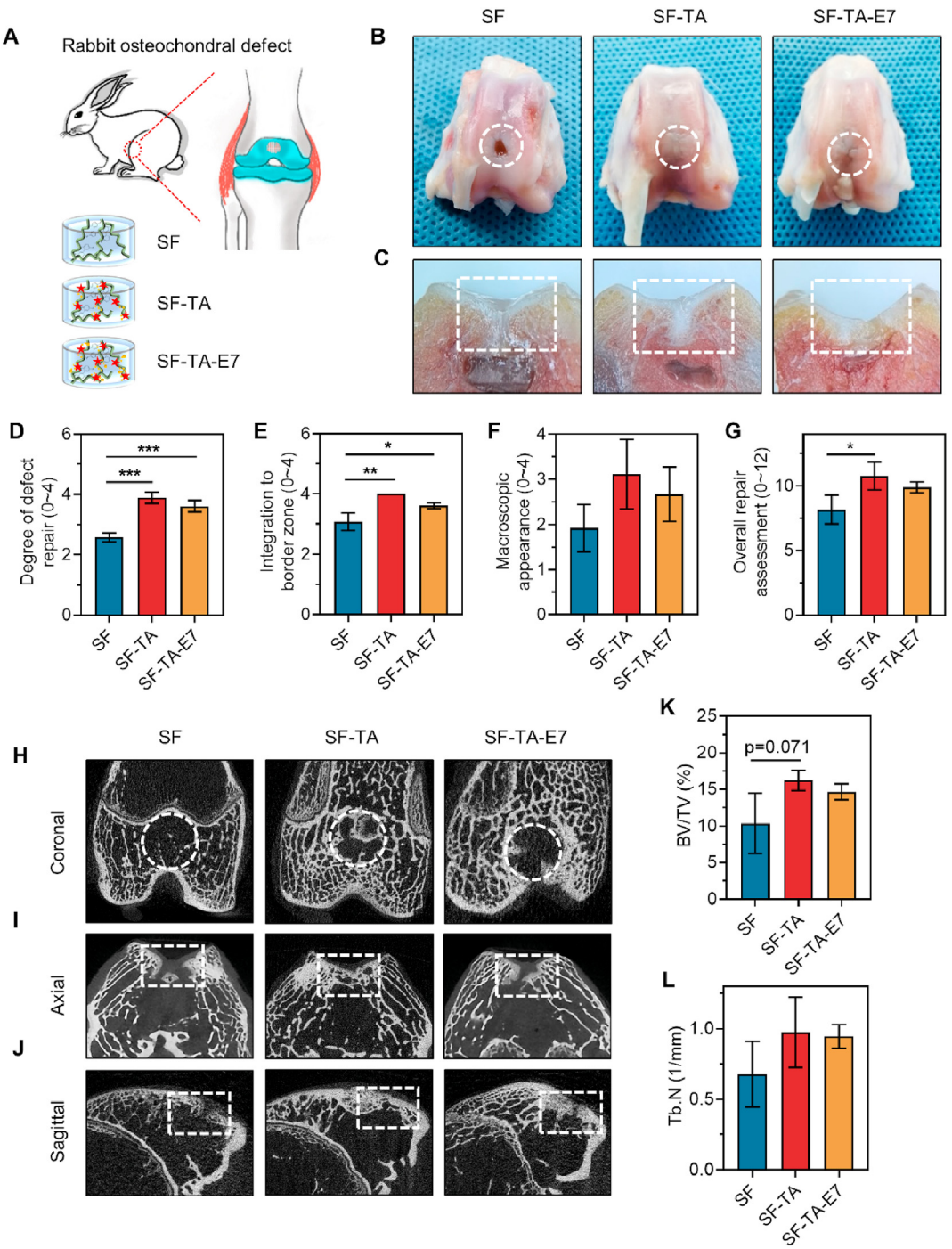

Fig. 5. Macroscopic and Micro-CT evaluation of SF-TA hydrogel into osteochondral defect at 12 weeks after implantation. (A) Schematic illustration of the animal model. (B) Gross morphology of joint specimens in the three groups collected at 12 weeks postoperatively. (C) Cross-sectional views of osteochondral repair at 12 weeks postoperatively. (D–G) Quantitative sub-item scores of the three groups according to the ICRS scoring system. (H–J) Micro-CT images in coronal, axial, and sagittal planes. Quantitative analysis of the regenerated subchondral bone by micro-CT, including (K) BV/TV (%) and (L) Tb. N. The white dotted circles and boxes in (B–C) and (H–J) indicate the original defect borders. Results are shown as mean ± SD. *p < 0.05, **p < 0.01, ***p < 0.001.

TA-E7 vs SF) (Fig. 5E). The SF-TA group had a full score of 4.00, indicating that the repaired tissue was smoothly connected with the surrounding tissue (Fig. 5E). Through the previous measurement of hydrogel viscosity, it was observed that TA increased the viscosity of SF hydrogel (Fig. 1N), which facilitated the material to adhere to the tissue surface, thereby promoting the connection between the neo-tissue and the defect border [45]. Regarding the score for "macroscopic appearance", there was no significant difference in the visual observation scores of the repaired surface among the three groups (Fig. 5F). For the "overall repair assessment" score, the repaired SF-TA group had the highest average score (10.78 ± 1.07), which was significantly higher than that of the SF group (8.17 ± 1.13, $p < 0.05$, Fig. 5G).

Subsequently, the regeneration of subchondral bone was evaluated by micro-CT. The two-dimensional reconstruction images in the coronal plane (Fig. 5H), axial plane (Fig. 5I), and sagittal plane (Fig. 5J) showed that SF-TA group and SF-TA-E7 group had more bone tissue formed in the defect area as compared to SF group. The bone structural parameters, including BV/TV and Tb. N were obtained from micro-CT scanning

images (Fig. 5K-L). Among the three groups, SF-TA group had the highest BV/TV (16.23 ± 1.38) and Tb. N (0.97 ± 0.25) values, while SF group had the lowest BV/TV (10.37 ± 4.10) and Tb. N (0.68 ± 0.23) values. The BV/TV (14.68 ± 1.08) and Tb. N (0.95 ± 0.084) of SF-TA-E7 group were slightly lower than those of SF-TA group, but no significant difference was detected.

Histological evaluation was further performed to evaluate the quality of the osteochondral defect repair (Fig. 6). In SF group, a large part of the cartilage and subchondral bone remained unrepaired (Fig. 6A). In contrast, the defects treated with SF-TA and SF-TA-E7 hydrogels were completely filled with newly-formed tissue which was smoothly integrated with the surrounding tissue both in the chondral and subchondral area (Fig. 6B and C). It can be seen from the cell morphology and ECM production that the newly-formed tissue in the chondral area of SF group was mainly composed of weakly stained fibrocartilage (Fig. 6D and G). On the contrary, the chondral area in the SF-TA and SF-TA-E7 groups had strong safranine-O and toluidine blue staining, indicating that the newly-formed tissue consisted mainly of hyaline cartilage (Fig. 6E and F, 6H–I). Typical round chondrocyte morphology and enhanced ECM production could be observed in the repaired cartilage tissue in the SF-TA and SF-TA-E7 groups, while mainly fibroblast morphology and less GAG was shown in the SF group (Fig. 6D–I). In the subchondral area, the repaired tissue of the SF group was mainly composed of loosely arranged fibrous tissue. In contrast, the SF-TA and SF-TA-E7 hydrogels promoted the enhanced regeneration of subchondral bone with abundant hyaline cartilage-like tissue and bony tissue (Fig. 6D–I). Furthermore, the histological score for cartilage evaluation showed that SF-TA (17.00 ± 2.65) and SF-TA-E7 (17.00 ± 2.00) groups had significantly enhanced scores than that of the SF group (7.33 ± 3.06, $p < 0.01$) (Fig. 6J). SF-TA-E7 group showed the highest subchondral bone score, but no significant difference was detected among all groups (Fig. 6K). Regarding the histological total score, the SF-TA-E7 group showed the highest score (31.00 ± 4.36) which was significantly higher than that of the SF group (13.67 ± 6.81, $p < 0.05$). Also, the histological total score of SF-TA group (29.33 ± 4.16)

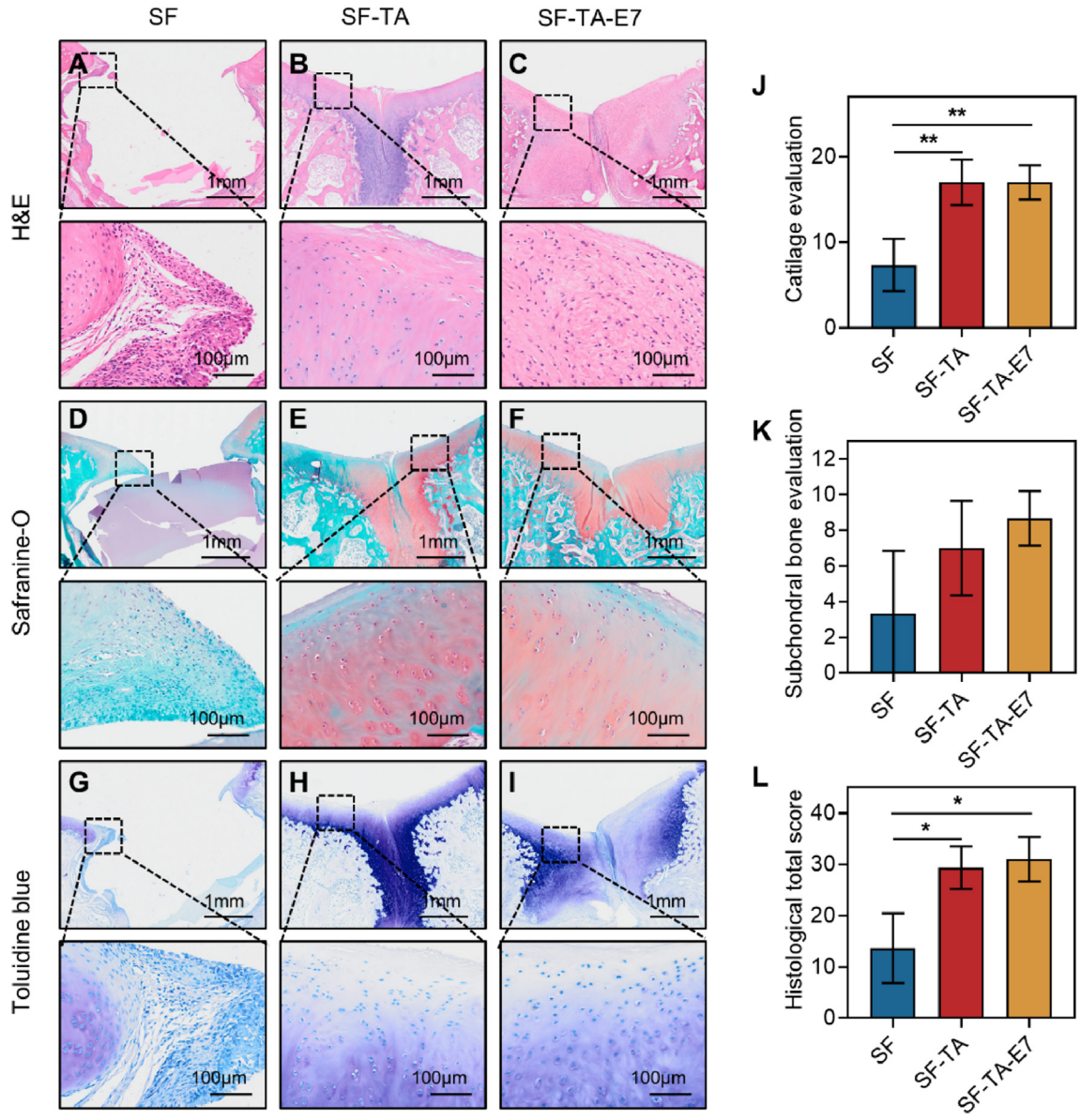

Fig. 6. Histological evaluation of SF-TA hydrogel into osteochondral defect at 12 weeks after implantation. (A–C) H&E staining, (D–F) safranine-O staining, and (G–I) toluidine blue staining of the regenerated osteochondral tissue at 12 weeks after implantation. The lower panels represent higher magnification images (scale bars = 100 μm) of the corresponding black dotted boxes in the upper panels (scale bars = 1 mm). (J) Cartilage sub-score, (K) subchondral bone sub-score, and (L) histological total score of the repaired tissue according to the established histological scoring system. Results are shown as mean ± SD. *$p < 0.05$, **$p < 0.01$.

was significantly higher than that of SF group ($p < 0.05$) (Fig. 6L).

The results of the animal studies collectively indicate that compared with SF hydrogel, SF-TA and SF-TA-E7 hydrogels have a superior repair effect on osteochondral defects, highlighting the vital role of TA in the repair process. Due to the lack of bioactivity of SF biomaterials, unfunctionalized SF scaffolds are inadequate to support osteochondral regeneration [5,77]. TA as a bioactive molecule, can alleviate oxidative stress by scavenging ROS, maintain cell viability and promote cell proliferation, thereby modifying the local unfavorable microenvironment of repair following osteochondral defects and enhancing tissue regeneration. We and other groups have previously reported that E7-functionalized scaffolds (hydrogel, porous matrix, or 3D printed scaffold) outperformed the unfunctionalized scaffolds with enhanced reparative efficacy in the treatment of osteochondral defects [25,32,78,79]. Indeed, in the current study, it was observed that SF-E7 hydrogel (i.e. E7-incorporated SF hydrogel) had better repair performance compared to the unfunctionalized hydrogel (SF hydrogel) (Fig. 6 and S5). However, the repair efficacy of SF-E7 hydrogel was inferior to that of the TA-functionalized hydrogels (SF-TA and SF-TA-E7 hydrogels) (Fig. 6 and S5), and SF-TA and SF-TA-E7 hydrogels showed comparable regenerative effect on osteochondral defects, suggesting that TA is more effective than E7 in the promotion of osteochondral regeneration. A possible explanation for this is that during osteochondral repair, recruiting BMSCs by pro-migratory molecules is not a crucial step since endogenous BMSCs can themselves migrate into the defect site. In contrast, providing a suitable microenvironment for reducing the harmful effects of ROS thereby maintaining cell viability and promoting cell proliferation, play a more important role in the repair of osteochondral defects, which is achieved by the incorporation of the bioactive TA molecule into the hydrogel.

It has been reported that the increased ROS reduces osteogenic and chondrogenic differentiation of MSCs [10,50]. However, in our study, the SF-TA hydrogel did not significantly improve the osteogenic and chondrogenic capacity of BMSCs (Fig. S3). In addition, the proteomic data indicated that SF-TA hydrogel had no significant effect on osteogenesis or chondrogenesis-related proteins or pathways (Figs. 3–4). Therefore, the enhancement effect of SF-TA hydrogel on osteochondral regeneration is mainly due to its suppression of oxidative stress by eliminating ROS, thereby maintaining cell viability and promoting cell proliferation, rather than directly promoting the dual-lineage differentiation of BMSCs. In the future, we may be able to load other types of peptides, such as osteoinductive and chondroinductive factors to improve BMSCs differentiation in the SF-TA hydrogel to achieve better repair effects [25,32]. In addition, we also found that in the SF-TA group, the regeneration of subchondral bone is not complete, which may be related to the weak mechanical properties of the hydrogels. Indeed, the high mechanical strength of the scaffold can improve stem cell-mediated bone regeneration [80]. We have recently developed a SF-laponite hydrogel, in which laponite as a nanoclay can increase its mechanical properties and dual-lineage bioactivity of the hydrogel [5]. The incorporation of laponite into the current SF-TA hydrogel will be considered in our future studies.

4. Conclusions

In conclusion, this study fabricated a multifunctional polyphenol-based SF hydrogel to alleviate oxidative stress and provide a supportive microenvironment for osteochondral regeneration. The SF-TA hydrogel with a supramolecular crosslinking structure exhibited enhanced viscosity and hydrophilicity beneficial for osteochondral regeneration, as well as a multitude of biological effects to eliminate ROS, protect BMSCs from oxidative stress-induced cell death, and sustain drug delivery. Notably, the proteomic analysis indicated that SF-TA hydrogel suppressed oxidative stress, which in turn improved cell proliferation in multiple proliferation and apoptosis-related pathways. When implanted into rabbit osteochondral defects, SF-TA hydrogel significantly facilitated simultaneous regeneration of both cartilage and subchondral bone at 12 weeks after in vivo implantation. Thus, the SF-TA hydrogel developed in this study provides a suitable microenvironment for osteochondral regeneration. Since the materials (SF and TA) used in this hydrogel have been approved by FDA, the SF-TA hydrogel shows great promise for future clinical treatment of osteochondral defects.

Credit author statement

Wei Zhang: Conceptualization, Methodology, Data curation, Formal analysis, Funding acquisition, Project administration, Writing – original draft, Writing- Reviewing and Editing. Yanan Zhang: Data curation, Formal analysis, Investigation. Xiaolong Li: Data curation, Formal analysis, Investigation, Software. Zhicheng Cao: Data curation, Formal analysis, Software. Qingyun Mo: Data curation, Visualization. Renwang Sheng: Data curation, Formal analysis. Chen Ling: Data curation. Jiayu Chi: Data curation. Qingqiang Yao: Funding acquisition, Resources. Jialin Chen: Funding acquisition, Writing- Reviewing and Editing. Hongmei Wang: Formal analysis, Funding acquisition, Writing – original draft, Writing- Reviewing and Editing.

Data availability

The data that support the findings of this study are available from the corresponding author upon reasonable request.

Declaration of competing interest

The authors declare that they have no known competing financial interests or personal relationships that could have appeared to influence the work reported in this paper.

Acknowledgements

This work was financially supported by the National Natural Science Foundation of China (81901903, 5171101275, 82072400), the Natural Science Foundation of Jiangsu Province (BK20190356, BK20190354, BK20200001), and the Zhishan Scholars Programs of Southeast University.

Appendix A. Supplementary data

Supplementary data to this article can be found online at https://doi.org/10.1016/j.mtbio.2022.100251.

References

[1] E.R. Vina, C.K. Kwoh, Epidemiology of osteoarthritis: literature update, Curr. Opin. Rheumatol. 30 (2) (2018) 160–167.
[2] C. Slattery, C.Y. Kweon, Classifications in brief: outerbridge classification of chondral lesions, Clin. Orthop. Relat. Res. 476 (10) (2018) 2101–2104.
[3] S.R. Goldring, M.B. Goldring, Changes in the osteochondral unit during osteoarthritis: structure, function and cartilage-bone crosstalk, Nat. Rev. Rheumatol. 12 (11) (2016) 632–644.
[4] W. Zhang, J. Chen, J. Tao, C. Hu, L. Chen, H. Zhao, G. Xu, B.C. Heng, H.W. Ouyang, The promotion of osteochondral repair by combined intra-articular injection of parathyroid hormone-related protein and implantation of a bi-layer collagen-silk scaffold, Biomaterials 34 (25) (2013) 6046–6057.
[5] W. Zhang, Y. Zhang, A. Zhang, C. Ling, R. Sheng, X. Li, Q. Yao, J. Chen, Enzymatically crosslinked silk-nanosilicate reinforced hydrogel with dual-lineage bioactivity for osteochondral tissue engineering, Mater. Sci. Eng. C 127 (2021) 112215.
[6] J. Yang, Y.S. Zhang, K. Yue, A. Khademhosseini, Cell-laden hydrogels for osteochondral and cartilage tissue engineering, Acta Biomater. 57 (2017) 1–25.
[7] P. Lepetsos, A.G. Papavassiliou, ROS/oxidative stress signaling in osteoarthritis, Biochim. Biophys. Acta 1862 (4) (2016) 576–591.
[8] J.A. Bolduc, J.A. Collins, R.F. Loeser, Reactive oxygen species, aging and articular cartilage homeostasis, Free Radic. Biol. Med. 132 (2019) 73–82.
[9] W.K. Kim, V. Meliton, N. Bourquard, T.J. Hahn, F. Parhami, Hedgehog signaling and osteogenic differentiation in multipotent bone marrow stromal cells are inhibited by oxidative stress, J. Cell. Biochem. 111 (5) (2010) 1199–1209.

[10] J. Mateos, A. De la Fuente, I. Lesende-Rodriguez, P. Fernandez-Pernas, M.C. Arufe, F.J. Blanco, Lamin A deregulation in human mesenchymal stem cells promotes an impairment in their chondrogenic potential and imbalance in their response to oxidative stress, Stem Cell Res. 11 (3) (2013) 1137–1148.
[11] R.L. Auten, J.M. Davis, Oxygen toxicity and reactive oxygen species: the devil is in the details, Pediatr. Res. 66 (2) (2009) 121–127.
[12] Z. Hao, Z. Song, J. Huang, K. Huang, A. Panetta, Z. Gu, J. Wu, The scaffold microenvironment for stem cell based bone tissue engineering, Biomater. Sci. 5 (8) (2017) 1382–1392.
[13] B. Kundu, R. Rajkhowa, S.C. Kundu, X. Wang, Silk fibroin biomaterials for tissue regenerations, Adv. Drug Deliv. Rev. 65 (4) (2013) 457–470.
[14] W. Huang, S. Ling, C. Li, F.G. Omenetto, D.L. Kaplan, Silkworm silk-based materials and devices generated using bio-nanotechnology, Chem. Soc. Rev. 47 (17) (2018) 6486–6504.
[15] S. Wei, J.X. Ma, L. Xu, X.S. Gu, X.L. Ma, Biodegradable materials for bone defect repair, Mil. Med. Res. 7 (1) (2020) 54.
[16] L. Zhang, W. Zhang, Y. Hu, Y. Fei, H. Liu, Z. Huang, C. Wang, D. Ruan, B.C. Heng, W. Chen, W. Shen, Systematic review of silk scaffolds in musculoskeletal tissue engineering applications in the recent decade, ACS Biomater. Sci. Eng. 7 (3) (2021) 817–840.
[17] Y.P. Singh, J.C. Moses, N. Bhardwaj, B.B. Mandal, Injectable hydrogels: a new paradigm for osteochondral tissue engineering, J. Mater. Chem. B 6 (35) (2018) 5499–5529.
[18] S. Park, S. Edwards, S. Hou, R. Boudreau, R. Yee, K.J. Jeong, A multi-interpenetrating network (IPN) hydrogel with gelatin and silk fibroin, Biomater. Sci. 7 (4) (2019) 1276–1280.
[19] Y. Zhang, Y. Cao, L. Zhang, H. Zhao, T. Ni, Y. Liu, Z. An, M. Liu, R. Pei, Fabrication of an injectable BMSC-laden double network hydrogel based on silk fibroin/PEG for cartilage repair, J. Mater. Chem. B 8 (27) (2020) 5845–5848.
[20] X. He, X. Liu, J. Yang, H. Du, N. Chai, Z. Sha, M. Geng, X. Zhou, C. He, Tannic acid-reinforced methacrylated chitosan/methacrylated silk fibroin hydrogels with multifunctionality for accelerating wound healing, Carbohydr. Polym. 247 (2020) 116689.
[21] W. Shi, Y. Kong, Y. Su, M.A. Kuss, X. Jiang, X. Li, J. Xie, B. Duan, Tannic acid-inspired, self-healing, and dual stimuli responsive dynamic hydrogel with potent antibacterial and anti-oxidative properties, J. Mater. Chem. B 9 (35) (2021) 7182–7195.
[22] Z. Guo, W. Xie, J. Lu, X. Guo, J. Xu, W. Xu, Y. Chi, N. Takuya, H. Wu, L. Zhao, Tannic acid-based metal phenolic networks for bio-applications: a review, J. Mater. Chem. B 9 (20) (2021) 4098–4110.
[23] S.A. Abouelmagd, F. Meng, B.K. Kim, H. Hyun, Y. Yeo, Tannic acid-mediated surface functionalization of polymeric nanoparticles, ACS Biomater. Sci. Eng. 2 (12) (2016) 2294–2303.
[24] Z. Qiao, X. Lv, S. He, S. Bai, X. Liu, L. Hou, J. He, D. Tong, R. Ruan, J. Zhang, J. Ding, H. Yang, A mussel-inspired supramolecular hydrogel with robust tissue anchor for rapid hemostasis of arterial and visceral bleedings, Bioact. Mater. 6 (9) (2021) 2829–2840.
[25] W. Zhang, C. Ling, H.Y. Liu, A.N. Zhang, L. Mao, J. Wang, J. Chao, L.J. Backman, Q.Q. Yao, J.L. Chen, Tannic acid-mediated dual peptide-functionalized scaffolds to direct stem cell behavior and osteochondral regeneration, Chem. Eng. J. 396 (2020) 125232.
[26] S.M. Bai, X.L. Zhang, P.Q. Cai, X.W. Huang, Y.Q. Huang, R. Liu, M.Y. Zhang, J.B. Song, X.D. Chen, H.H. Yang, A silk-based sealant with tough adhesion for instant hemostasis of bleeding tissues, Nanoscale Horiz. 4 (6) (2019) 1333–1341.
[27] J. Jing, S. Liang, Y. Yan, X. Tian, X. Li, Fabrication of hybrid hydrogels from silk fibroin and tannic acid with enhanced gelation and antibacterial activities, ACS Biomater. Sci. Eng. 5 (9) (2019) 4601–4611.
[28] X.J. Gao, Q.Y. Dai, L.T. Yao, H. Dong, Q.T. Li, X.D. Cao, A medical adhesive used in a wet environment by blending tannic acid and silk fibroin, Biomater Sci-Uk 8 (9) (2020) 2694–2701.
[29] Z. Man, L. Yin, Z. Shao, X. Zhang, X. Hu, J. Zhu, L. Dai, H. Huang, L. Yuan, C. Zhou, H. Chen, Y. Ao, The effects of co-delivery of BMSC-affinity peptide and rhTGF-beta1 from coaxial electrospun scaffolds on chondrogenic differentiation, Biomaterials 35 (19) (2014) 5250–5260.
[30] J. Wu, L. Cao, Y. Liu, A. Zheng, D. Jiao, D. Zeng, X. Wang, D.L. Kaplan, X. Jiang, Functionalization of silk fibroin electrospun scaffolds via BMSC affinity peptide grafting through oxidative self-polymerization of dopamine for bone regeneration, ACS Appl. Mater. Interfaces 11 (9) (2019) 8878–8895.
[31] D.N. Rockwood, R.C. Preda, T. Yucel, X. Wang, M.L. Lovett, D.L. Kaplan, Materials fabrication from Bombyx mori silk fibroin, Nat. Protoc. 6 (10) (2011) 1612–1631.
[32] W. Zhang, C. Ling, A. Zhang, H. Liu, Y. Jiang, X. Li, R. Sheng, Q. Yao, J. Chen, An all-silk-derived functional nanosphere matrix for sequential biomolecule delivery and in situ osteochondral regeneration, Bioact. Mater. 5 (4) (2020) 832–843.
[33] B.P. Partlow, C.W. Hanna, J. Rnjak-Kovacina, J.E. Moreau, M.B. Applegate, K.A. Burke, B. Marelli, A.N. Mitropoulos, F.G. Omenetto, D.L. Kaplan, Highly tunable elastomeric silk biomaterials, Adv. Funct. Mater. 24 (29) (2014) 4615–4624.
[34] I.R. Serra, R. Fradique, M.C. Vallejo, T.R. Correia, S.P. Miguel, I.J. Correia, Production and characterization of chitosan/gelatin/beta-TCP scaffolds for improved bone tissue regeneration, Mater. Sci. Eng. C Mater. Biol. Appl. 55 (2015) 592–604.
[35] X. Wang, T. Yucel, Q. Lu, X. Hu, D.L. Kaplan, Silk nanospheres and microspheres from silk/pva blend films for drug delivery, Biomaterials 31 (6) (2010) 1025–1035.
[36] K. Wang, Y. Wang, S. Lin, X. Liu, S. Yang, G.S. Jones, Analysis of DPPH inhibition and structure change of corn peptides treated by pulsed electric field technology, J. Food Sci. Technol. 52 (7) (2015) 4342–4350.
[37] S.J. Humphrey, O. Karayel, D.E. James, M. Mann, High-throughput and high-sensitivity phosphoproteomics with the EasyPhos platform, Nat. Protoc. 13 (9) (2018) 1897–1916.
[38] M.P. van den Borne, N.J. Raijmakers, J. Vanlauwe, J. Victor, S.N. de Jong, J. Bellemans, D.B. Saris, S. International, Cartilage repair, international cartilage repair society (ICRS) and oswestry macroscopic cartilage evaluation scores validated for use in autologous chondrocyte implantation (ACI) and microfracture, Osteoarthritis Cartilage 15 (12) (2007) 1397–1402.
[39] Y. Jiang, L. Chen, S. Zhang, T. Tong, W. Zhang, W. Liu, G. Xu, R.S. Tuan, B.C. Heng, R. Crawford, Y. Xiao, H.W. Ouyang, Incorporation of bioactive polyvinylpyrrolidone-iodine within bilayered collagen scaffolds enhances the differentiation and subchondral osteogenesis of mesenchymal stem cells, Acta Biomater. 9 (9) (2013) 8089–8098.
[40] S. Liu, R. Chen, C.H. Hagedorn, Tannic acid inhibits hepatitis C virus entry into Huh7.5 cells, PLoS One 10 (7) (2015), e0131358.
[41] J. Wang, H.S. Xiao, Y.Y. Zhu, S.P. Liu, Z.H. Yuan, J. Wu, L.X. Wen, Tannic acid induces the mitochondrial pathway of apoptosis and S phase Arrest in porcine intestinal IPEC-J2 cells, Toxins 11 (7) (2019) 397.
[42] N. Abbasi, S. Hamlet, R.M. Love, N.-T. Nguyen, Porous scaffolds for bone regeneration, J. Sci.: Adv. Device Mater. 5 (1) (2020) 1–9.
[43] T. Li, X. Hu, Q. Zhang, Y. Zhao, P. Wang, X. Wang, B. Qin, W. Lu, Poly(acrylic acid)-chitosan @ tannic acid double-network self-healing hydrogel based on ionic coordination, Polym. Adv. Technol. 31 (7) (2020) 1648–1660.
[44] L. Brazdaru, M. Micutz, T. Staicu, M. Albu, D. Sulea, M. Leca, Structural and rheological properties of collagen hydrogels containing tannic acid and chlorhexidine digluconate intended for topical applications, Cr Chim 18 (2) (2015) 160–169.
[45] F.F. Zhou, Y. Hong, X.Z. Zhang, L. Yang, J. Li, D.M. Jiang, V. Bunpetch, Y.J. Hu, H.W. Ouyang, S.F. Zhang, Tough hydrogel with enhanced tissue integration and in situ forming capability for osteochondral defect repair, Appl. Mater. Today 13 (2018) 32–44.
[46] L. Pan, H. Wang, C. Wu, C. Liao, L. Li, Tannic-acid-coated polypropylene membrane as a separator for lithium-ion batteries, ACS Appl. Mater. Interfaces 7 (29) (2015) 16003–16010.
[47] M. Korkmaz, R. Turkmen, H.H. Demirel, Z.K. Saritas, Effect of boron on the repair of osteochondral defect and oxidative stress in rats: an experimental study, Biol. Trace Elem. Res. 187 (2) (2019) 425–433.
[48] X. Liu, Y. Xu, S. Chen, Z. Tan, K. Xiong, Y. Li, Y. Ye, Z.P. Luo, F. He, Y. Gong, Rescue of proinflammatory cytokine-inhibited chondrogenesis by the antiarthritic effect of melatonin in synovium mesenchymal stem cells via suppression of reactive oxygen species and matrix metalloproteinases, Free Radic. Biol. Med. 68 (2014) 234–246.
[49] Z. Shao, X. Zhang, Y. Pi, X. Wang, Z. Jia, J. Zhu, L. Dai, W. Chen, L. Yin, H. Chen, C. Zhou, Y. Ao, Polycaprolactone electrospun mesh conjugated with an MSC affinity peptide for MSC homing in vivo, Biomaterials 33 (12) (2012) 3375–3387.
[50] C.S. Lee, H.S. Hwang, S. Kim, J. Fan, T. Aghaloo, M. Lee, Inspired by nature: facile design of nanoclay-organic hydrogel bone sealant with multifunctional properties for robust bone regeneration, Adv. Funct. Mater. 30 (43) (2020) 2003717.
[51] N. Schwartz, A. Verma, C.B. Bivens, Z. Schwartz, B.D. Boyan, Rapid steroid hormone actions via membrane receptors, Biochim. Biophys. Acta 1863 (9) (2016) 2289–2298.
[52] Z.P. Howard, A. Omsland, Selective inhibition of coxiella burnetii replication by the steroid hormone progesterone, Infect. Immun. 88 (12) (2020) e00894-19.
[53] S.R. Burger, Current regulatory issues in cell and tissue therapy, Cytotherapy 5 (4) (2003) 289–298.
[54] L. You, Z. Wang, H. Li, J. Shou, Z. Jing, J. Xie, X. Sui, H. Pan, W. Han, The role of STAT3 in autophagy, Autophagy 11 (5) (2015) 729–739.
[55] K. Baek, D.T. Krist, J.R. Prabu, S. Hill, M. Klugel, L.M. Neumaier, S. von Gronau, G. Kleiger, B.A. Schulman, NEDD8 nucleates a multivalent cullin-RING-UBE2D ubiquitin ligation assembly, Nature 578 (7795) (2020) 461–466.
[56] F. Rahman, J.L. Johnson, J. Zhang, J. He, K. Pestonjamasp, S. Cherqui, S.D. Catz, DYNC1LI2 regulates localization of the chaperone-mediated autophagy receptor LAMP2A and improves cellular homeostasis in cystinosis, Autophagy (2021) 1–19.
[57] H. Ghozlan, A. Showalter, E. Lee, X. Zhu, A.R. Khaled, Chaperonin-Containing TCP1 complex (CCT) promotes breast cancer growth through correlations with key cell cycle regulators, Front. Oncol. 11 (2021) 663877.
[58] A.R. Kim, K.W. Choi, TRiC/CCT chaperonins are essential for organ growth by interacting with insulin/TOR signaling in Drosophila, Oncogene 38 (24) (2019) 4739–4754.
[59] N. Tang, X. Cai, L. Peng, H. Liu, Y. Chen, TCP1 regulates Wnt7b/beta-catenin pathway through P53 to influence the proliferation and migration of hepatocellular carcinoma cells, Signal Transduct. Targeted Ther. 5 (1) (2020) 169.
[60] Y. Guo, X. Cang, L. Zhu, M. Zhu, A. Li, Z. Wang, Y. Zhang, X. Wang, E. Song, PPP1CA/YAP/GS/Gln/mTORC1 pathway activates retinal Muller cells during diabetic retinopathy, Exp. Eye Res. 210 (2021) 108703.
[61] D.K. Dube, S. Dube, L. Abbott, O. Elsekaily, J.W. Sanger, J.M. Sanger, B.J. Poiesz, Sarcomeric TPM3 expression in human heart and skeletal muscle, Cytoskeleton (Hoboken) 77 (8) (2020) 313–328.
[62] Y. Ma, H. Zhang, X. Yang, Y. Li, J. Guan, Y. Lv, H. Li, Y. Liu, Z. Gai, Establishment of a human induced pluripotent stem cell line (SDQLCHi004-A) from a patient with nemaline myopathy-4 disease carrying heterozygous mutation in TPM2 gene, Stem Cell Res. 40 (2019) 101559.
[63] M.Y. Kimura, K. Hayashizaki, K. Tokoyoda, S. Takamura, S. Motohashi, T. Nakayama, Crucial role for CD69 in allergic inflammatory responses: CD69-Myl9 system in the pathogenesis of airway inflammation, Immunol. Rev. 278 (1) (2017) 87–100.

[64] M.Y. Kimura, R. Koyama-Nasu, R. Yagi, T. Nakayama, A new therapeutic target: the CD69-Myl9 system in immune responses, Semin. Immunopathol. 41 (3) (2019) 349–358.
[65] G.A. Hobbs, B. Zhou, A.D. Cox, S.L. Campbell, Rho GTPases, oxidation, and cell redox control, Small GTPases 5 (2014), e28579.
[66] S. Rezatabar, A. Karimian, V. Rameshknia, H. Parsian, M. Majidinia, T.A. Kopi, A. Bishayee, A. Sadeghinia, M. Yousefi, M. Monirialamdari, B. Yousefi, RAS/MAPK signaling functions in oxidative stress, DNA damage response and cancer progression, J. Cell. Physiol. 234 (9) (2019) 14951–14965.
[67] S. Hartmann, A.J. Ridley, S. Lutz, The function of rho-associated kinases ROCK1 and ROCK2 in the pathogenesis of cardiovascular disease, Front. Pharmacol. 6 (2015).
[68] K. Miyagawa, M. Shi, P.I. Chen, J.K. Hennigs, Z. Zhao, M. Wang, C.G. Li, T. Saito, S. Taylor, S. Sa, A. Cao, L. Wang, M.P. Snyder, M. Rabinovitch, Smooth muscle contact drives endothelial regeneration by BMPR2-Notch1-mediated metabolic and epigenetic changes, Circ. Res. 124 (2) (2019) 211–224.
[69] M. Knobloch, S.M. Braun, L. Zurkirchen, C. von Schoultz, N. Zamboni, M.J. Arauzo-Bravo, W.J. Kovacs, O. Karalay, U. Suter, R.A. Machado, M. Roccio, M.P. Lutolf, C.F. Semenkovich, S. Jessberger, Metabolic control of adult neural stem cell activity by Fasn-dependent lipogenesis, Nature 493 (7431) (2013) 226–230.
[70] M. Roudaut, S. Idriss, A. Caillaud, A. Girardeau, A. Rimbert, B. Champon, A. David, A. Leveque, L. Arnaud, M. Pichelin, X. Prieur, A. Prat, N.G. Seidah, K. Zibara, C. Le May, B. Cariou, K. Si-Tayeb, PCSK9 regulates the NODAL signaling pathway and cellular proliferation in hiPSCs, Stem Cell Rep. 16 (12) (2021) 2958–2972.
[71] S. Khiati, S.A. Baechler, V.M. Factor, H. Zhang, S.Y. Huang, I. Dalla Rosa, C. Sourbier, L. Neckers, S.S. Thorgeirsson, Y. Pommier, Lack of mitochondrial topoisomerase I (TOP1mt) impairs liver regeneration, in: Proceedings of the National Academy of Sciences of the United States of America, vol. 112, 2015, pp. 11282–11287, 36.
[72] L. Huangfu, Q. He, J. Han, J. Shi, X. Li, X. Cheng, T. Guo, H. Du, W. Zhang, X. Gao, F. Luan, X. Xing, J. Ji, MicroRNA-135b/CAMK2D Axis contribute to malignant progression of gastric cancer through EMT process remodeling, Int. J. Biol. Sci. 17 (8) (2021) 1940–1952.
[73] H. Wang, Z. Jin, T. Pei, W. Song, Y. Gong, D. Chen, L. Zhang, M. Zhang, G. Zhang, Long noncoding RNAs C2dat1 enhances vascular smooth muscle cell proliferation and migration by targeting MiR-34a-5p, J. Cell. Biochem. 120 (3) (2019) 3001–3008.
[74] M.J. Ellis, L. Ding, D. Shen, J. Luo, V.J. Suman, J.W. Wallis, B.A. Van Tine, J. Hoog, R.J. Goiffon, T.C. Goldstein, S. Ng, L. Lin, R. Crowder, J. Snider, K. Ballman, J. Weber, K. Chen, D.C. Koboldt, C. Kandoth, W.S. Schierding, J.F. McMichael, C.A. Miller, C. Lu, C.C. Harris, M.D. McLellan, M.C. Wendl, K. DeSchryver, D.C. Allred, L. Esserman, G. Unzeitig, J. Margenthaler, G.V. Babiera, P.K. Marcom, J.M. Guenther, M. Leitch, K. Hunt, J. Olson, Y. Tao, C.A. Maher, L.L. Fulton, R.S. Fulton, M. Harrison, B. Oberkfell, F. Du, R. Demeter, T.L. Vickery, A. Elhammali, H. Piwnica-Worms, S. McDonald, M. Watson, D.J. Dooling, D. Ota, L.W. Chang, R. Bose, T.J. Ley, D. Piwnica-Worms, J.M. Stuart, R.K. Wilson, E.R. Mardis, Whole-genome analysis informs breast cancer response to aromatase inhibition, Nature 486 (7403) (2012) 353–360.
[75] A. Yoshimi, K.T. Lin, D.H. Wiseman, M.A. Rahman, A. Pastore, B. Wang, S.C. Lee, J.B. Micol, X.J. Zhang, S. de Botton, V. Penard-Lacronique, E.M. Stein, H. Cho, R.E. Miles, D. Inoue, T.R. Albrecht, T.C.P. Somervaille, K. Batta, F. Amaral, F. Simeoni, D.P. Wilks, C. Cargo, A.M. Intlekofer, R.L. Levine, H. Dvinge, R.K. Bradley, E.J. Wagner, A.R. Krainer, O. Abdel-Wahab, Coordinated alterations in RNA splicing and epigenetic regulation drive leukaemogenesis, Nature 574 (7777) (2019) 273–277.
[76] M. Pavel, M. Renna, S.J. Park, F.M. Menzies, T. Ricketts, J. Fullgrabe, A. Ashkenazi, R.A. Frake, A.C. Lombarte, C.F. Bento, K. Franze, D.C. Rubinsztein, Contact inhibition controls cell survival and proliferation via YAP/TAZ-autophagy axis, Nat. Commun. 9 (1) (2018) 2961.
[77] F. Zhou, X. Zhang, D. Cai, J. Li, Q. Mu, W. Zhang, S. Zhu, Y. Jiang, W. Shen, S. Zhang, H.W. Ouyang, Silk fibroin-chondroitin sulfate scaffold with immuno-inhibition property for articular cartilage repair, Acta Biomater. 63 (2017) 64–75.
[78] H. Huang, X. Zhang, X. Hu, Z. Shao, J. Zhu, L. Dai, Z. Man, L. Yuan, H. Chen, C. Zhou, Y. Ao, A functional biphasic biomaterial homing mesenchymal stem cells for in vivo cartilage regeneration, Biomaterials 35 (36) (2014) 9608–9619.
[79] W. Shi, M. Sun, X. Hu, B. Ren, J. Cheng, C. Li, X. Duan, X. Fu, J. Zhang, H. Chen, Y. Ao, Structurally and functionally optimized silk-fibroin–gelatin scaffold using 3D printing to repair cartilage injury in vitro and in vivo, Adv. Mater. 29 (29) (2017) 1701089.
[80] H. Sun, F. Zhu, Q. Hu, P.H. Krebsbach, Controlling stem cell-mediated bone regeneration through tailored mechanical properties of collagen scaffolds, Biomaterials 35 (4) (2014) 1176–1184.